Spring 5-19-2017

Numerical Determination of Critical Mach number of a Three-Element Airfoil in Unbounded Flow and in Ground Effect

Bowen Hu
Washington University in St. Louis

Recommended Citation

Hu, Bowen, "Numerical Determination of Critical Mach number of a Three-Element Airfoil in Unbounded Flow and in Ground Effect" (2017). *Engineering and Applied Science Theses & Dissertations*. 263.
https://openscholarship.wustl.edu/eng_etds/263

WASHINGTON UNIVERSITY IN ST. LOUIS

School of Engineering and Applied Science

Department of Mechanical Engineering and Material Science

Thesis Examination Committee:

Ramesh Agarwal, Chair

Qiulin Qu

Swami Karunamoorthy

Numerical Determination of Critical Mach number of a Three-Element Airfoil in Unbounded
Flow and in Ground Effect

by
Bowen Hu

A thesis presented to
the School of Engineering and applied Science
of Washington University in
partial fulfillment of the
requirements for the degree
of Master of Science

May 2017
St. Louis, Missouri

Table of Contents

iii

List of Figures

List of Tables

<u>Acknowledgments</u>

First of all, I would like to thank my advisor Dr. Ramesh Agarwal. I have learned a lot of professional knowledge from him in aerodynamics and computational fluid dynamics. More importantly, his patience and persistence in providing research guidance have deeply touched me. For me, Dr. Ramesh Agarwal is not only a professor but also a mentor in my life.

I would also like to thank everyone who helped me with the thesis. Thanks to Dr. Qiulin Qu for his guidance in my research and his continuous encouragement. Thanks to Junhui Li for his patience in answering my questions. Thanks to Boshun Gao for the help he provided when I met with problems in my research. Thanks to Ning Deng and Pan Du for helping me with the mesh generation. Thanks to Xu Han for teaching me how to set parameter in the simulations. I am also thankful to all my colleagues in CFD lab for their continuous help and good company.

Finally, I would like to acknowledge my committee members, Dr. Peters and Dr. Karunarmoorthy, for taking the time to read the thesis and attend its defense.

<div align="right">Bowen Hu</div>

Washington University in St. Louis

May 2017

Dedicated to my parents

I want to dedicate this thesis to my parents (Yingzhong Hu and Qun Wang) and grandparents for their life-time guidance, love and support.

ABSTRACT OF THE THESIS

Numerical Determination of Critical Mach number on a Three-Element Airfoil in Unbounded

Flow and in Ground Effect

by

Bowen Hu

Master of Science in Department of Mechanical Engineering and Material Science

Washington University in St. Louis, 2017

Research Advisor: Professor Ramesh Agarwal

The critical Mach number is an important property of airfoils on aerodynamics. When the

freestream Mach number exceeds the critical Mach number, shock will appear on the aircraft and

cause a huge loss of energy. Lift decreases sharply and drag increases dramatically. We usually

hope to increase the critical Mach number and delay the occurrence of shock so that the aircraft

can fly with a higher speed and carry more weight.

In this thesis, the main task is to determine the critical Mach number of multi-element airfoil

30P30N in unbounded flow and in ground effect. Commercial software ICEM is employed to

generate mesh. ANSYS Fluent is conducted to compute flow filed. The compressible The

Reynolds-averaged Navier - Stokes equations (or RANS equations) with the Spalart-Allmaras

Turbulence Model are solved in flow field. The results are discussed in three parts. Firstly the

results lead to the determination of the critical Mach number of 30P30N airfoil in unbounded

flow and compare it with the critical Mach number of single element airfoil RAE2822. In

addition, the evolution of aerodynamics of 30P30N airfoil from unbounded flow to ground effect is displayed and the reasons are analyzed. Finally, the determination of the critical Mach number at different ride heights in ground effect is shown and a clear change in the critical Mach number can be seen.

.

Chapter 1: Introduction

This chapter provides the background of the Computational Fluid Dynamics simulation of flow past a three-element 30P30N airfoil and the motivation behind this research on determination of critical Mach number of 30P30N airfoil. The scope of the thesis is also included.

1.1 Motivation

McDonnell Douglas 30P30N three-element airfoil is one of the most widely used airfoil multi-element configuration by the CFD workers. It is a typical landing configuration. In 1993, 30P30N airfoil was used as a challenging configuration for CFD validation at CFD Challenge Workshop held at NASA Langley [1]. Because of the availability of excellent experimental data, the critical Mach number of an airfoil is always of vital concern in aircraft design. Since then, this configuration has been studied by many researchers for validation of CFD code worldwide. For a free-stream Mach number greater than the critical Mach number, shocks appear on the airfoil resulting in a dramatic increases in the drag. By optimizing the shape of airfoil, it may be possible to increase the critical Mach number and delay the appearance of shocks. One way to increase the critical Mach number is to have a swept wing, it can decrease effective speed of aircraft, so higher speed is needed to produce a shock. Another way is to design a variable sweep aircraft, which can change the wing sweep angle according to the flight speed. In the low-speed take-off and landing, smaller sweep angle is used so that the lift in front wing increases; at high subsonic and supersonic speed, large sweep angle is used to improve the aircraft's acceleration and high speed flight performance.

1.2 Brief Review of Literature

In the past many decades, the aerodynamics and flow physics of a single-element airfoil in unbounded flow and ground effect have been widely studied and are well understood. Coullietter and Plotkin [2] used the numerical and analytical methods to study the airfoils with zero thickness and non-zero thickness in ground effect. For the zero thickness airfoil, as the camber ratio and angle of attack increases, the lift at a given ground height decreases; for the non-zero thickness airfoil, the lift increases when the thickness ratio increases. Hsiun and Chen [3] studied the influence of camber and thickness on the aerodynamics of a 2D airfoil in ground effect by numerical method. They compared the aerodynamic results of single element NACA0006, NACA0009, NACA0012, NACA2412 and NACA4412 airfoils at different angles of attacks and ride heights and concluded that the aerodynamic forces are determined by the shape of the passage between the lower surface of the airfoil and the ground. Qu et al. [4] investigated the flow physics and aerodynamics of a NACA4412 airfoil in GE for a wide range of angel of attack α = -4 ~ 20° by numerical simulations. For low to moderate AOA, when the ride height is reduced, pressure on the lower surface of the airfoil increases. For high AOA, when the ride height is reduced, the adverse pressure gradient along the chord-wise direction increases resulting in a larger region of separated flow.

High-lift devices are widely used in modern aircrafts during take-off and landing. However, the research effort devoted to the study of GE of high-lift devices has been very limited. Yang et al. [5] reported numerical results for a three-element airfoil LIT2 (slat angle δs = 25° and flap angle δf = 20°) and a two-element airfoil (modified from L1T2) in GE. Their results indicated that the lifts of both the airfoils decreased gradually as the ride height was reduced, but the decrease was very small. Carter [6] studied the aerodynamic characteristics of an un-swept wing with an

2

aspect ratio of 10 and a taper ratio of 0.3. With the decreasing ride height, the lift curve slope of the wing with retraced flaps increased, but the maximum lift of the wing with full-span double-slotted flaps deflected 30 ° and 50 ° decreased.

1.3   Scope of the Thesis

Since the knowledge about the aerodynamics and flow physics of multi-element airfoils in ground effect has been very limited. Therefore in this thesis, the ground effect of a multi-element airfoil is studied with particular emphasison the critical Mach number. The critical Mach number of 30P30N airfoil in unbounded flow and in ground is determined by numerical simulation.

Chapter 2: Methodology

This section presents the methodology for flow field simulation of multi-element airfoil 30p30N.

2.1 Geometry and Mesh Generation

2.1.1 Geometry

The typical geometry of a high-lift airfoil from leading edge to trailing edge consists of three

parts: slat, main and flap. As shown in Fig.2.1.The location and orientation of the flap and slat

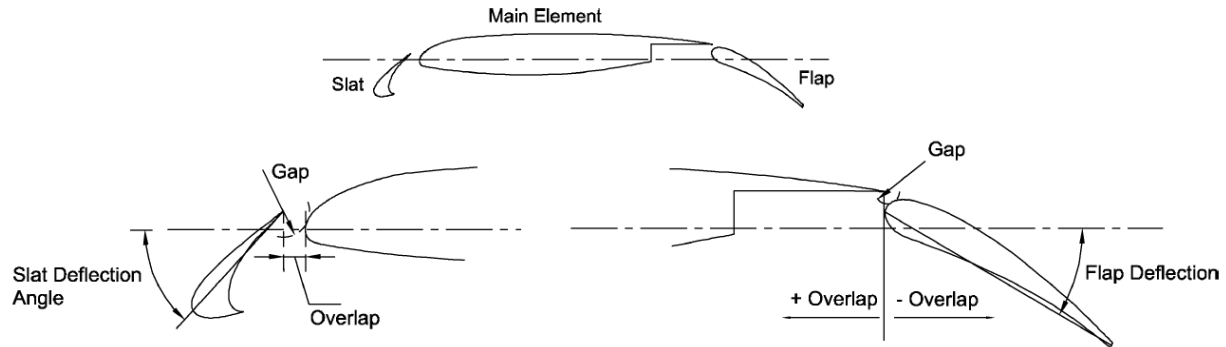are defined by the deflection angles, overlap and gap.[7]

Fig 2.1. Definitions of gap, overlap, and deflection angles in a three-element airfoil.

The 30P30N is a well-studied high-lift airfoil; geometric settings such as the gap and overhang

of the slat and the flap are summarized in Table 2.1 [8].

Table 2.1 Geometric parameters (gap and overhang values are specified as percentage of stowed chord, c).

Slat deflection angle	δs	30°
Flap deflection angle	δf	30°
Slat gap	gs	2.95%
Flap gap	gf	1.27%
Slat overhang	os	−2.5%
Flap overhang	of	0.25%

As shown in Figure 2.2, the angle of attack is referenced to the main element chord. The angle of attack used in the present cases is α=10°. Ride height h is defined as distance between the trailing edge of the flap and the ground.
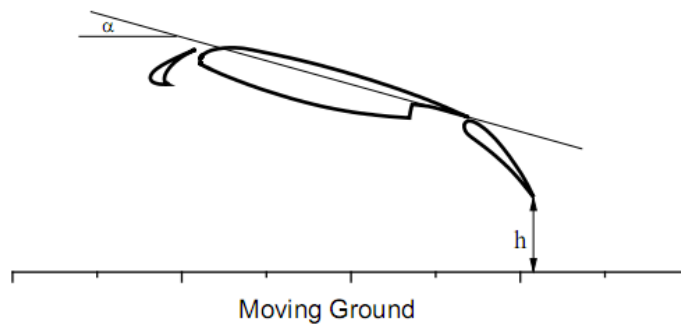

Fig. 2.2 Sketch of 30P30N airfoil in GE.

2.2 Mesh Generation

2.1.1 Unbounded Flow

Mesh is generated using the ICEM software in ANSYS. The rectangular computational domain and structured mesh layout for the unbounded flow field are shown in Fig 2.3. The inlet, outlet,

5

top and bottom boundaries are located at 40c away from the airfoil. They are all set as pressure far-field condition. The airfoil is set as a no-slip static wall condition.

Fig 2.3 Computational domain and structured mesh layout in unbounded flow

2.1.2 Ground Effect Flow Field

The semi-circular computational domain and structured mesh layout are generated for the ground effect flow field as shown in Fig 2.4. The inlet, outlet and top boundaries are located 40c away from the airfoil. They are all set as pressure far-field condi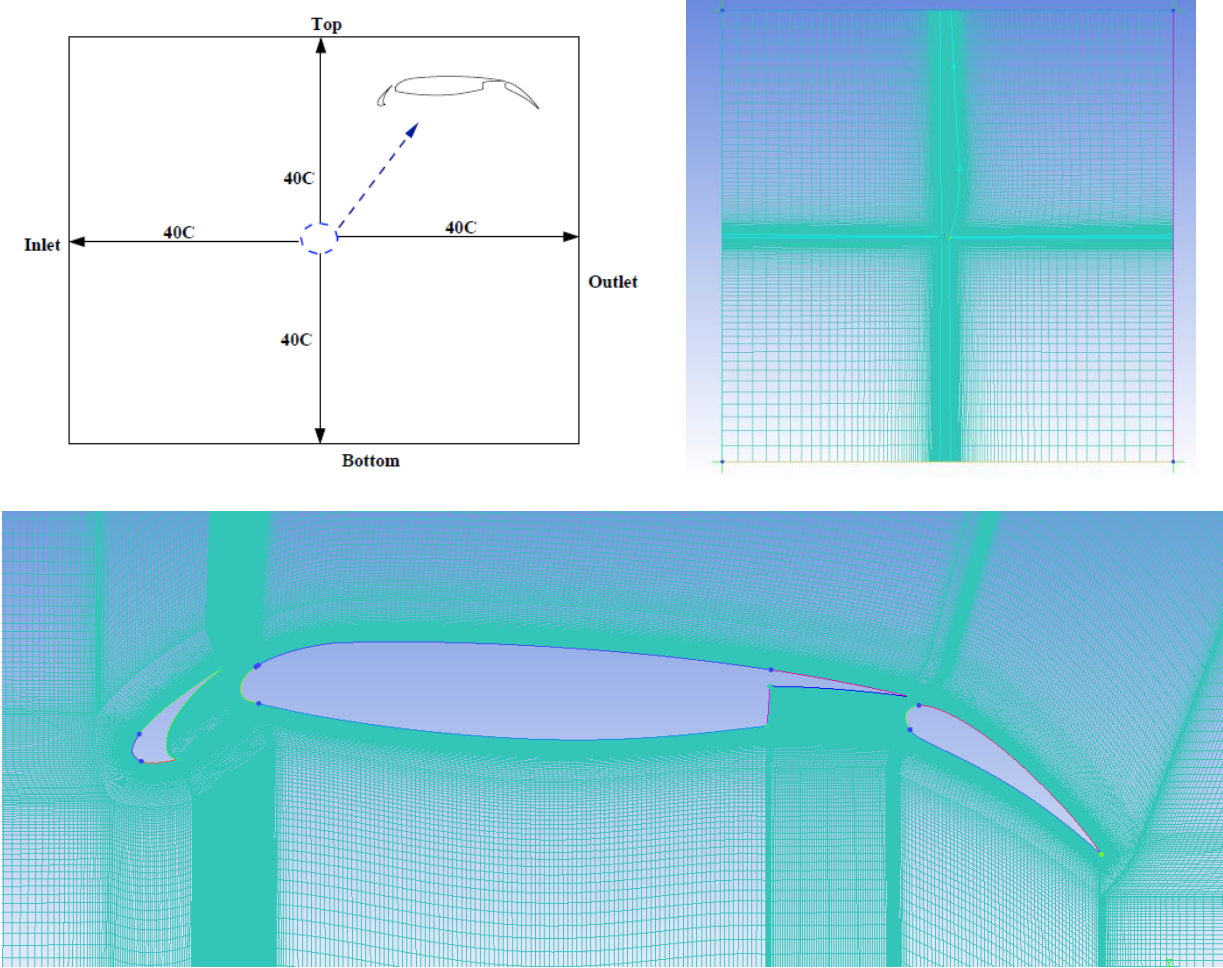tion. The bottom boundary is a no-slip moving wall condition with a translation velocity equal to the free-stream velocity. The distance

6

between the bottom boundary and the airfoil is changed as h/c=0.1, h/c=0.2 and h/c=1. The

airfoil is set as a no-slip static wall condition. The mesh is refined in the region between the

airfoil and the ground.
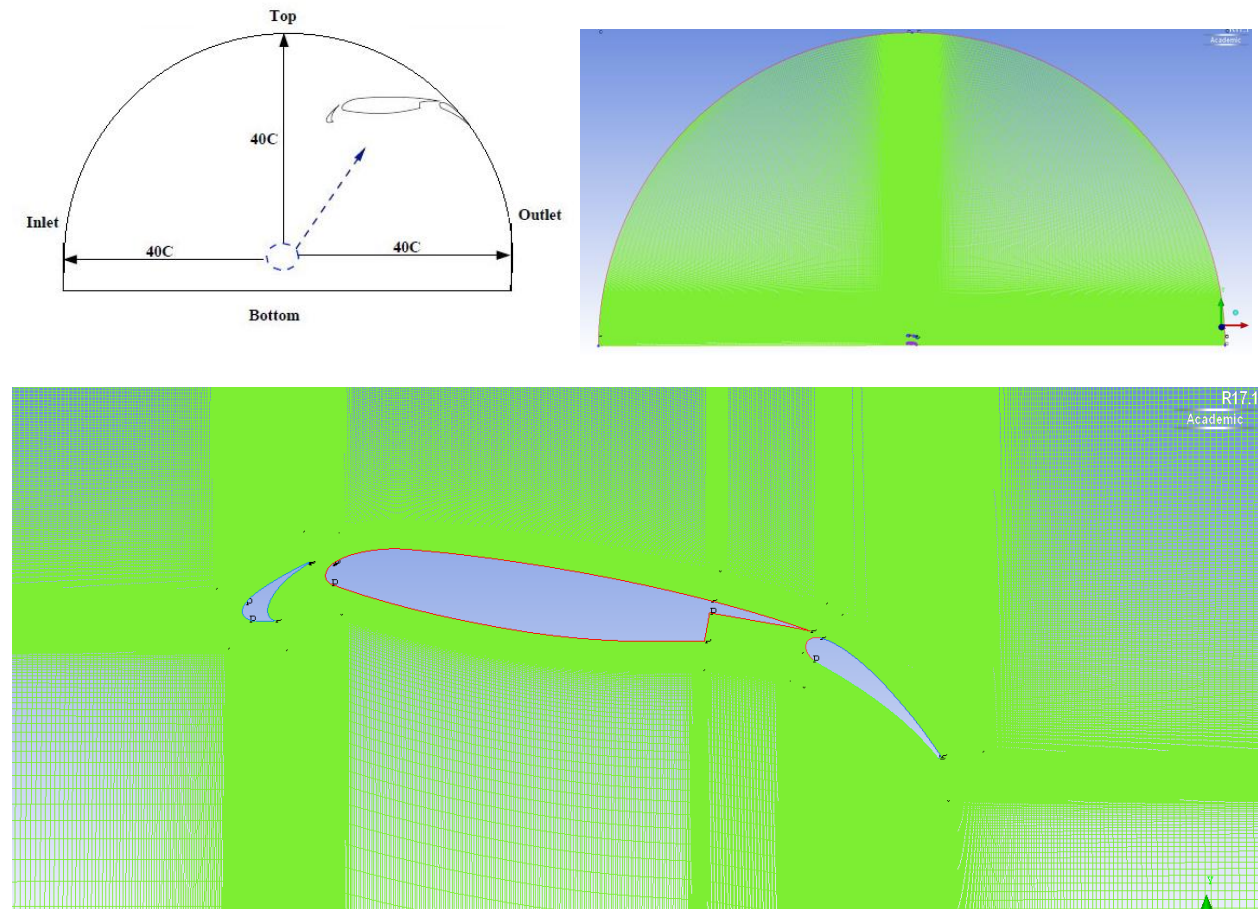
Fig 2.4 Computational domain and structured mesh layout in ground effect

2.3 Simulation Method

Reynolds-Averaged Navier-Stokes (RANS) equations are solved using the finite volume method.

Spalart-Allmaras (S-A) one-equation turbulence model is employed as described in section 2.4.

The double precision solver of the commercial CFD software ANSYS FLUENT 17.1 is

employed to conduct the numerical simulation. A second order upwind scheme is utilized for the

convection terms and a second order central difference scheme is used for the diffusion terms.

The SIMPLE algorithm is employed for the pressure-velocity coupling. The steady compressible

2.4 Turbulence Model

Spalart-Allmaras (SA) model is employed to solve the Reynolds-Averaged Navier-Stokes

(RANS) equations. The advantage of this model is simplicity and high accuracy [9] for

aerodynamic flows.

It is a one-equation model for transport written in terms of a eddy-viscosity-like term [10]. The

equation is written as:

$$\frac{\partial \hat{\nu}}{\partial t} + u_j \frac{\partial \hat{\nu}}{\partial x_j} = c_{b1}(1 - f_{t2})\hat{S}\hat{\nu} - \left[c_{w1}f_w - \frac{c_{b1}}{\kappa^2}f_{t2}\right]\left(\frac{\hat{\nu}}{d}\right)^2 + \frac{1}{\sigma}\left[\frac{\partial}{\partial x_j}\left((\nu + \hat{\nu})\frac{\partial \hat{\nu}}{\partial x_j}\right) + c_{b2}\frac{\partial \hat{\nu}}{\partial x_i}\frac{\partial \hat{\nu}}{\partial x_i}\right]$$

The eddy viscosity is related to the eddy viscosity term through the equation

$$\mu_t = \rho \hat{\nu} f_{v1}$$

where

$$f_{v1} = \frac{\chi^3}{\chi^3 + c_{v1}^3}$$

and

$$\chi = \frac{\hat{\nu}}{\nu}$$

The production term is given by

$$\hat{S} = \Omega + \frac{\hat{\nu}}{\kappa^2 d^2}f_{v2}$$

where Ω is the magnitude of the vorticity, d is the distance from the field point to the nearest

wall, and

8

$$f_{v2} = 1 - \frac{\chi}{1 + \chi f_{v1}}$$

The destruction function $f\omega$ is given by

$$f_w = g \left[\frac{1 + c_{w3}^6}{g^6 + c_{w3}^6} \right]^{1/6}$$

where

$$g = r + c_{w2}(r^6 - r)$$

and

$$r = min \left[\frac{\hat{\nu}}{\hat{S}\kappa^2 d^2}, 10 \right]$$

The transition functions are

$$f_{t1} = c_{t1}g_t \exp[-c_{t2}(\omega_t^2/\Delta U^2)(d^2 + g_t^2 d_t^2)]$$

$$f_{t2} = c_{t3}\exp(-c_{t4}\chi^2)$$

The constants used in model are

$$c_{b1} = 0.1355 \quad \sigma = 2/3 \quad c_{b2} = 0.622 \quad \kappa = 0.41$$

$$c_{w2} = 0.3 \quad c_{w3} = 2 \quad c_{v1} = 7.1 \quad c_{t3} = 1.2 \quad c_{t4} = 0.5$$

$$c_{w1} = \frac{c_{b1}}{\kappa^2} + \frac{1 + c_{b2}}{\sigma}$$

Chapter 3 Determination of Critical Mach Number in Unbounded Flow

3.1 Lift Coefficient and Drag Coefficient

Figures 3.1 and 3.2 show the change in lift coefficient and drag coefficient of 30P30N airfoil and RAE2822 airfoil respectively. One can see a clear increasing and then decreasing trend with Mach number in the lift curves. In drag curves, drag coefficient almost remain the same and then have a sharp increase with the Mach number. The reason is the presence of shock on the airfoil when Mach number exceeds the critical Mach number. In case of RAE2822 airfoil, which is a typical airfoil, both the lift coefficient and drag coefficient are smaller than 30P30N as expected. Since the multi-element airfoil has larger chord length and camber. In unbounded flow, for 30P30N airfoil, the larger chord length and camber will increase the lift from the potential flow point of view, and the flow in the gaps will further increase the lift by delaying the flow separation from viscous flow point of view. The critical Mach number of 30P30N is 0.33 at AOA=10 degree according to the simulation data, and the critical Mach number of RAE2822 airfoil is 0.75 at AOA=2.31 degree.
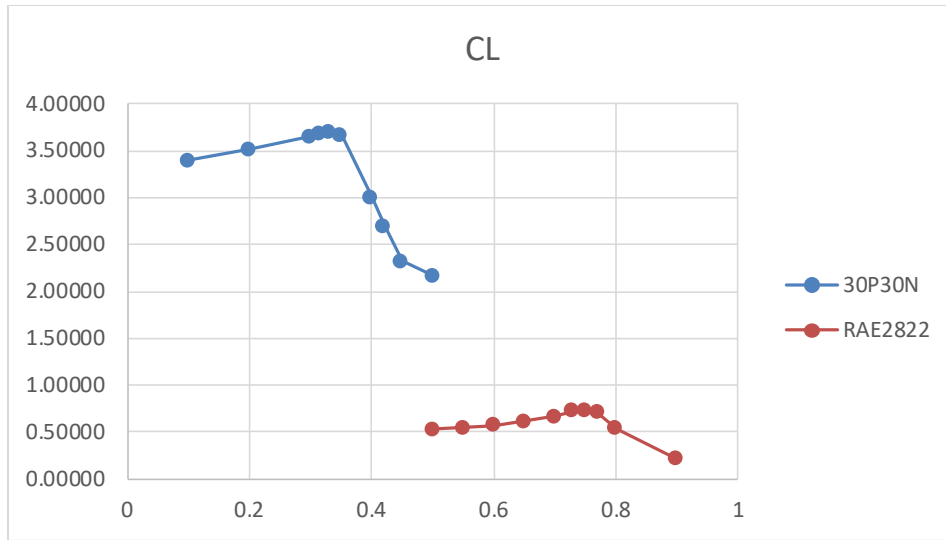
Fig 3.1 Variation of lift coefficients of 30P30N and RAE2822 airfoils in unbounded flow with Mach number
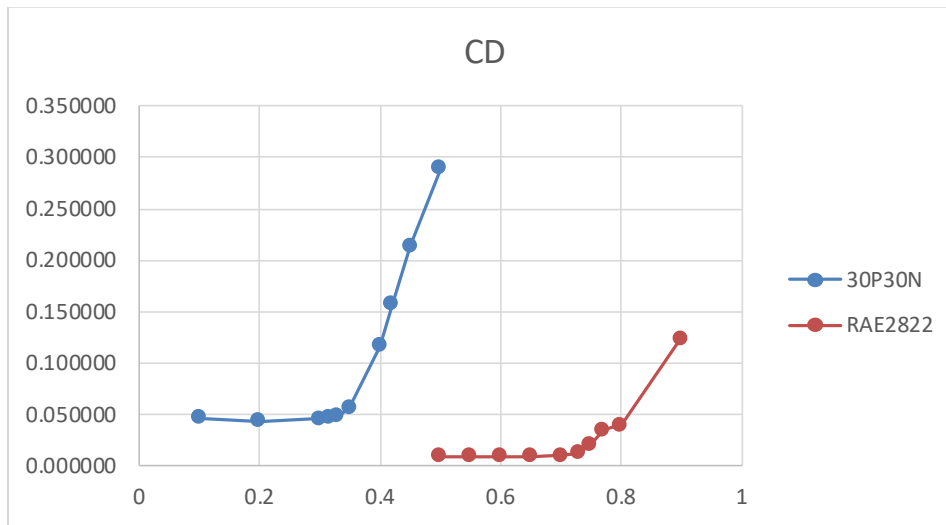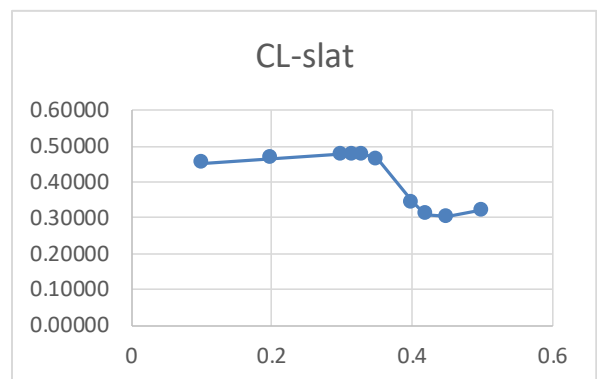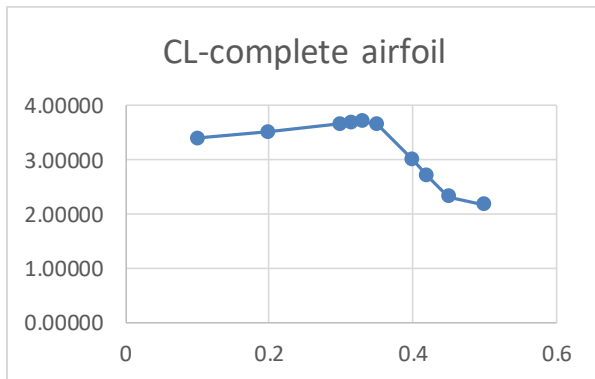

Fig 3.2 Variation of drag coefficients of 30P30N and RAE2822 airfoils in unbounded flow with Mach number
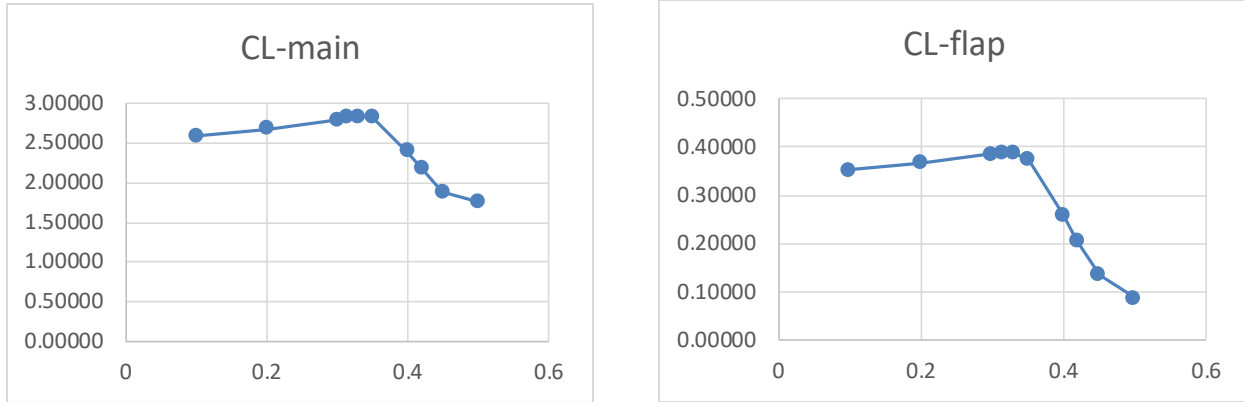

11

Fig 3.3 Variation of lift coefficients of complete airfoil, slat, main and flap of 30P30N with Mach number in unbounded flow

Fig 3.3 shows the change in lift coefficient of complete airfoil, slat, main and flap. The lift curves of main and flap show an increasing and then a decreasing trend in lift before and after the critical Mach number. The lift curve of slat however first increases in a small range and then decreases and finally increases as freestream Mach number increases. To conclude, the relative decrease in the lift of the main wing is the largest, and that of the slat is the smallest.
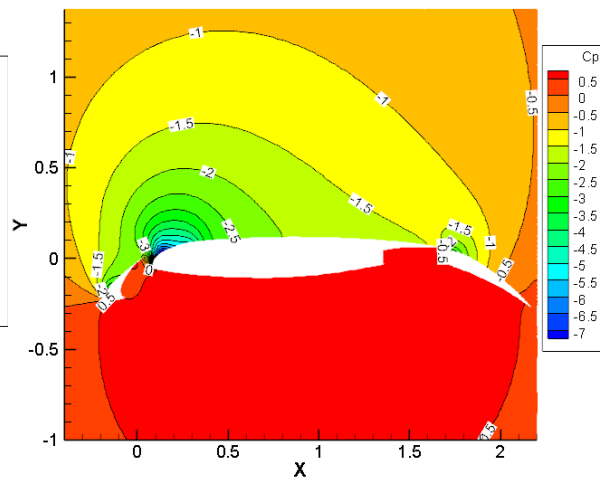
3.2 Pressure Coefficient Contours

Figure 3.4 shows the pressure coefficient contours of 30P30N airfoil at various Mach number before and after the critical Mach number of 0.33. The contours are shown for freestream Mach number = 0.2, 0.3 0.33, 0.35, 0.4 and 0.5. From Fig 3.4 (a) and Fig 3.4 (b), it can be seen that the pressure coefficients on lower surface of the airfoil are the same, however they are slightly different on the upper surface. When freestream Mach number increases from 0.2 to 0.3, the suction increases, and the pressure on the upper surface decreases. This leads to increase in the lift coefficient. As freestream Mach number increase from 0.3 Fig 3.4 (b) to 0.33 Figure 3.4 (c), so lift coefficient increases. As freestream Mach number increase from 0.33 Fig 3.4 (c) to 0.35 Figure 3.4 (d), the pressure coefficient on both the upper surface and lower surface decrease, lift coefficient decrease. Also, one can see that the pressure contours are no longer smooth, which

12

indicate a higher pressure gradient and a shock begins to appear. As freestream Mach number increse from 0.35 Fig 3.4 (d) to 0.4 Figure 3.4 (e), the change in pressure gradient is obvious. It can also be noticed that in the tail of the main part region and on the flap, there is sharp suction leading to decrease in lift. This is the main reason for lift coefficient to decrease sharply. It cann be seen from Fig 3.4 (e) to Fig 3.4 (f), pressure coefficient in the shock region decreases sharply, leading to increase in lift. Before the critical Mach number, there is no shock, thus drag remians nearly constant. After the critical Mach number, shock appears on the airfoil and creates a large pressure difference between upstream and downstream of the shock resulting in sharp increase in drag.
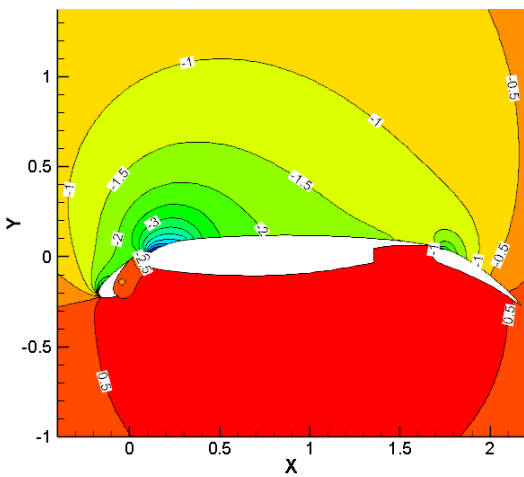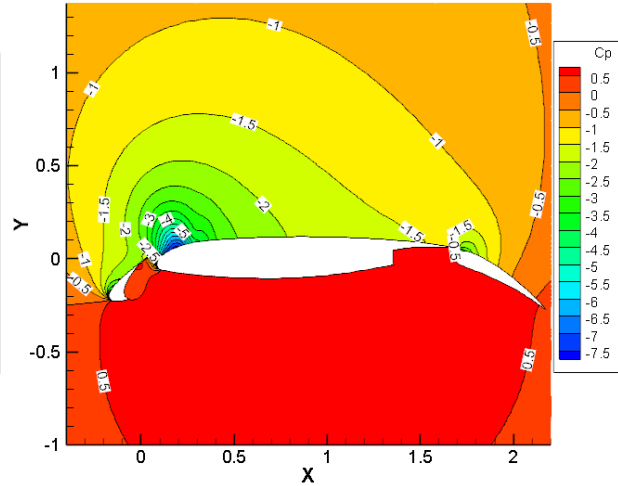

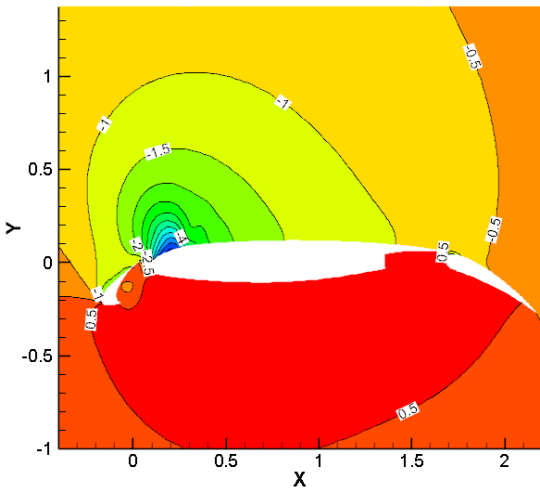(a) Freestream Mach number=0.2   (b) Freestream Mach number=0.3
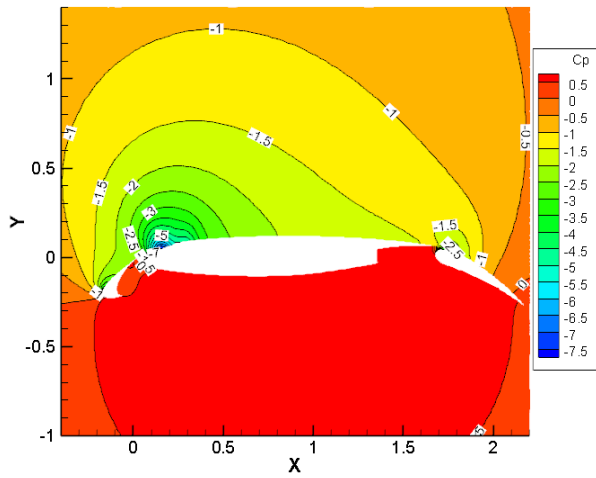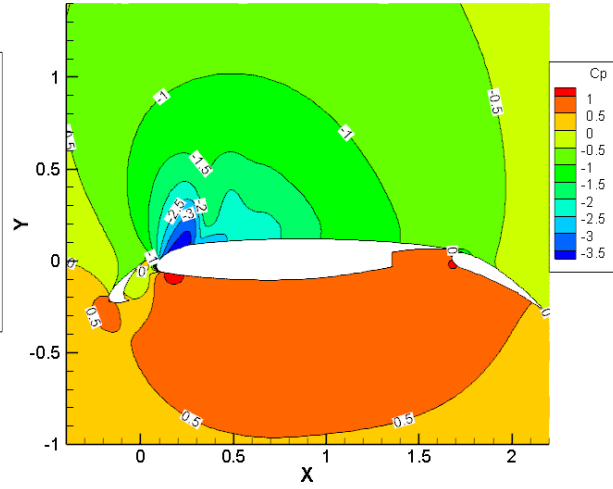
(c) Freestream Mach number=0.33   (d) Freestream Mach number=0.35
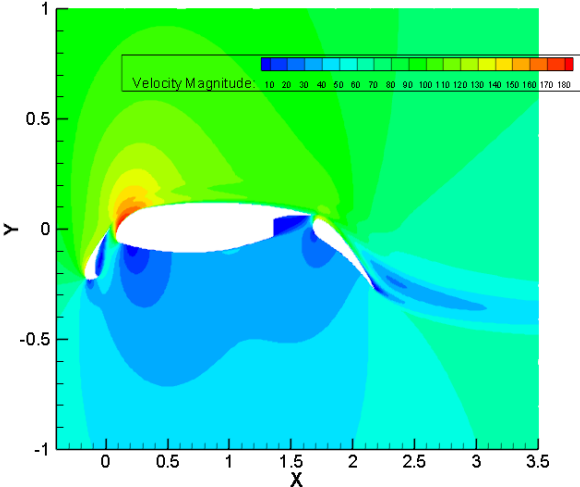

(e) Freestream Mach number=0.4   (f) Freestream Mach number=0.5

Fig 3.4 Pressure coefficient contours of 30P30N at freestream Mach number = 0.2, 0.3, 0.33, 0.35, 0.4 and 0.5
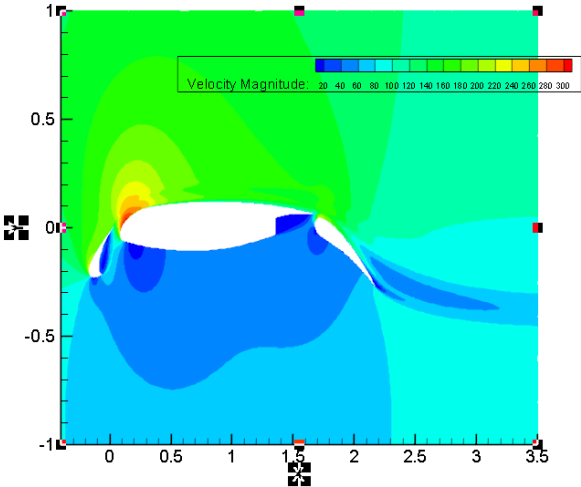
3.3 Velocity Magnitude Contours

Fig 3.5 shows the velocity magnitude contours around 30P30N airfoil at various Mach number before and after critical Mach number. The velocity on the lower surface of airfoil is obviously lower than that on the upper surface. According to the Bernoulli's Equation, when pressure becomes larger, the velocity becomes smaller. Hence the colors in velocity contour are opposite to the colors of pressure coefficient contours. From velocity magnitude contours, it can be seen

14

that there are three stagnation points located near leading bottom part of slat,the main wing and the flap. Also, near the leading upper surface of the slat, the main wing and the flap, the velocity is maximum. When freestream Mach number increases, the velocity magnitude increases, and the shock strength increase on the main part. There is a flow separation in the gap between the slat and the main wing and the gap between the main wing and the flap. As the Mach number becomes larger than the critical Mach number, flow separates on the upper surface of 30P30N airfoil as can be seen from the streamline plots in Figure 3.6.
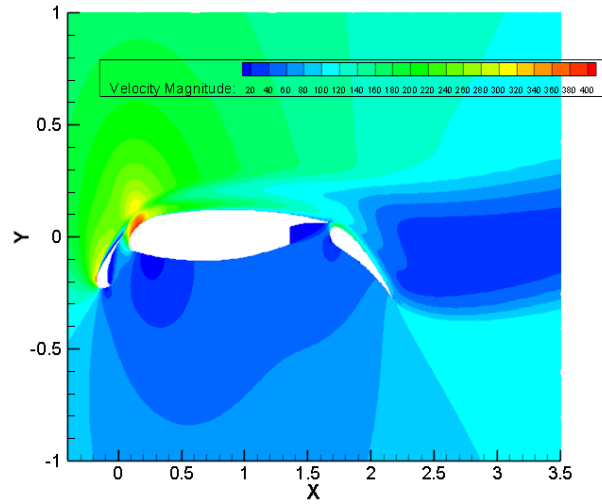

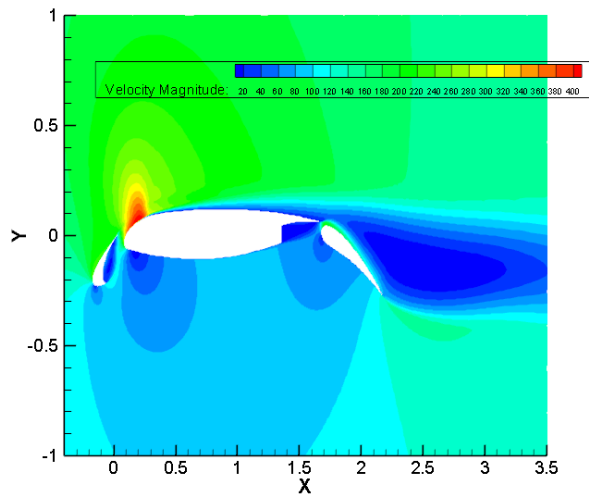(a) Freestream Mach number=0.2   (b) Freestream Mach number=0.3
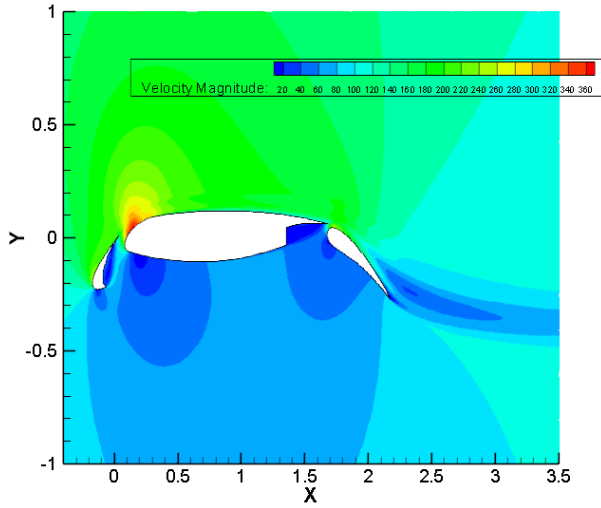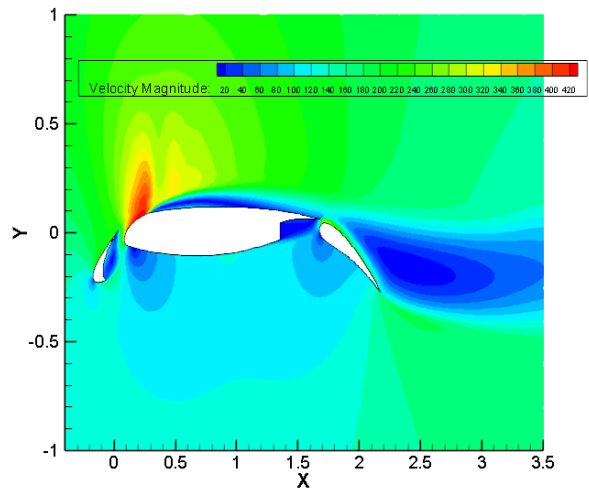
(c) Freestream Mach number=0.33

(d) Freestream Mach number=0.35

(e) Freestream Mach number=0.4

(f) Freestream Mach number=0.5

Fig 3.5 Velocity magnitude contours of 30P30N at freestream Mach number = 0.2, 0.3, 0.33, 0.35, 0.4 and 0.5

3.4 Streamlines

Figure 3.6 shows the streamlines around 30P30N airfoil at various Mach number before and after critical Mach number. The various colors stand represent the velocity magnitude of different streamlines. It can be seen that there are two regions of flow separations in the gap between slat and the main wing and the other in the gap between the main wing and the flap. There is large

16

area of separation behind the flap when freestream Mach number become greater than the critical

Mach number. It shows in the downstream of flap.

(a) Freestream Mach number=0.2
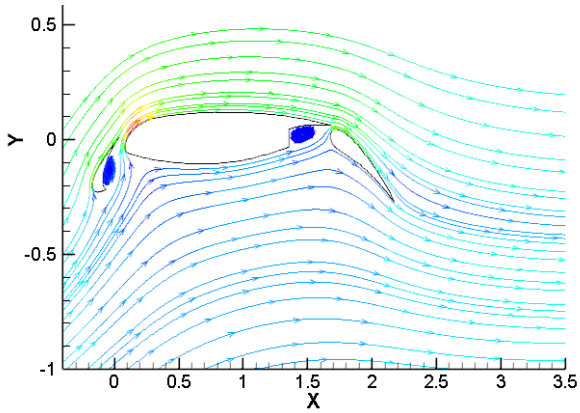
(b) Freestream Mach number=0.3

(c) Freestream Mach number=0.33

(d) Freestream Mach number=0.35
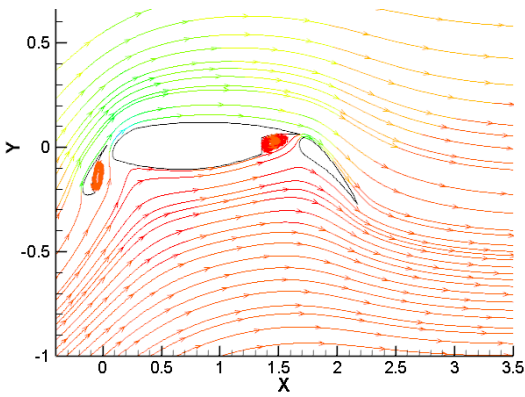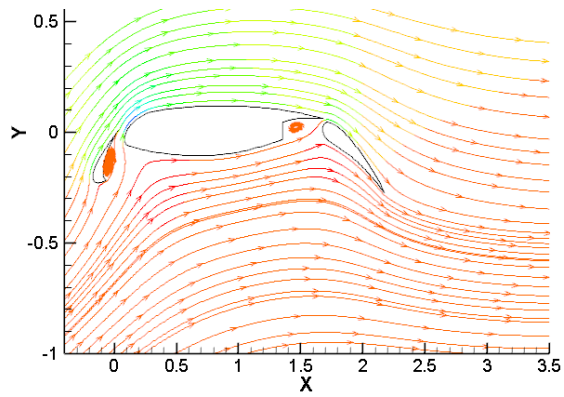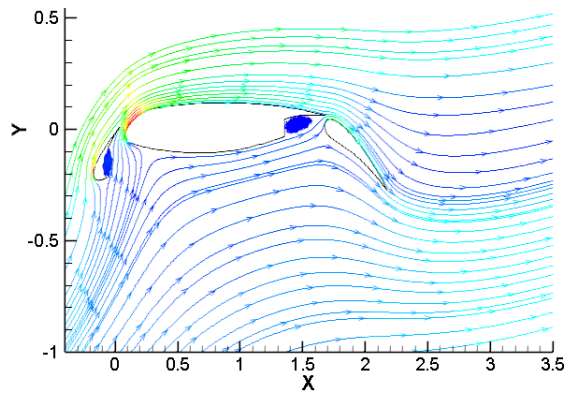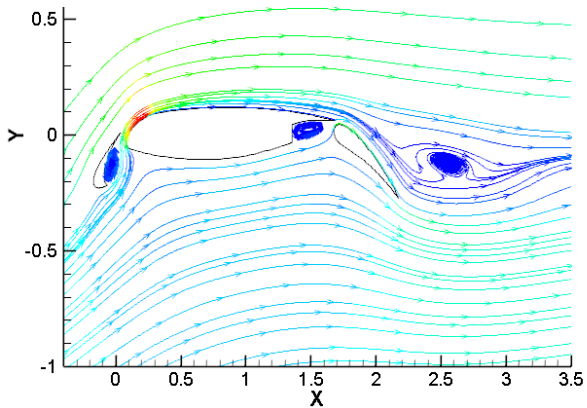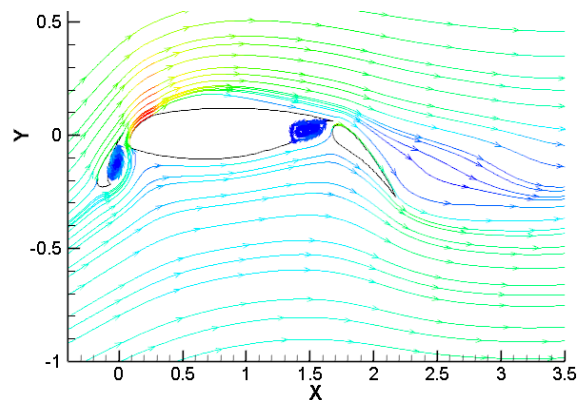
(e) Freestream Mach number=0.4

(f) Freestream Mach number=0.5

Fig 3.6 Streamlines around 30P30N at freestream Mach number = 0.2, 0.3, 0.33, 0.35, 0.4 and 0.5

3.5 Conclusions

Compared to a single-element airfoil like RAE2822, a multi-element airfoil has larger lift since it has larger chord length and camber, and has gaps. In the unbounded flow, the larger chord length and camber will increase the lift from the potential flow point of view, and the flow in the gaps will further increase the lift by delaying the flow separation from viscous flow point of view. For 30P30N airfoil has an increase in lift coefficient with Mach numbers less than the critical Mach number and decrease in lift coefficient with Mach numbers greater than the critical Mach number. The drag coefficient remain almost keeps the same at Mach numbers less than the critical Mach number and then has a sharp increase when freestream Mach number becomes larger than the critical Mach number due to the appearance of shock on the upper suraface. Pressure contours and velocity contours show the pressure and velocity distributions on the upper and lower surface of 30P30N which validate the conclusion about the lift and drag coefficients described above.

Chapter 4 Aerodynamics of 30P30N Airfoil in Ground Effect

When an object moves in the proximity to the ground, its flow field and aerodynamics change, this is called the ground effect. In this chapter, we determine the flow field and aerodynamics of 30P30N in ground effect various ride heights h/c=0.1, 0.2 and 1 by numerical simulation.

4.1 Lift Coefficient and Drag Coefficient

In order to discuss the change in the aerodynamics of 30P30N airfoil from unbounded flow to ground effect, we consider it flow field at different heights above the ground at the same freestream Mach number. Figure 4.1 and Figure 4.2 show the change in lift coefficient and drag coefficient respectively freestream for Mach number = 0.2 at different ride height h/c = 0.1, 0.2, 1 and ∞ (which is unbounded flow). There is an increasing trend in lift coefficient and drag coefficient when ground clearance increases.
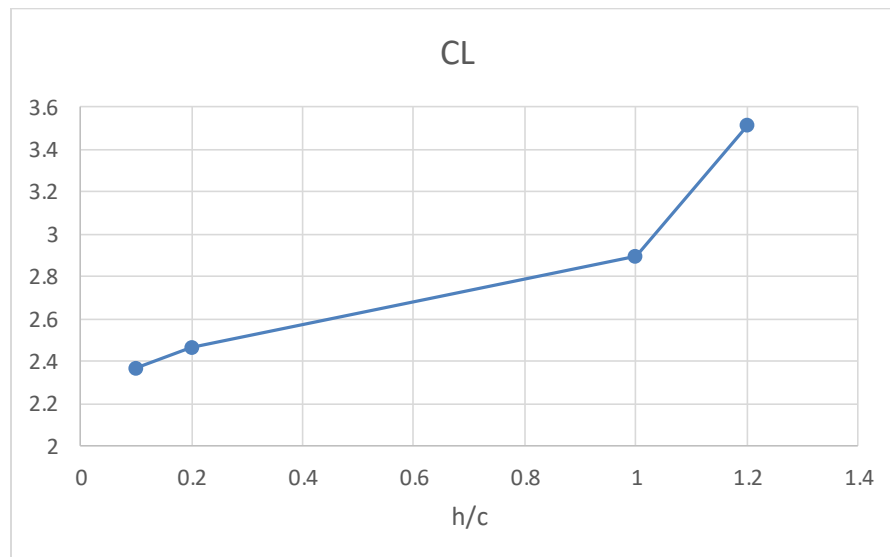

Fig 4.1 Lift coefficient of 30P30N at different ride heights at freestream Mach number = 0.2

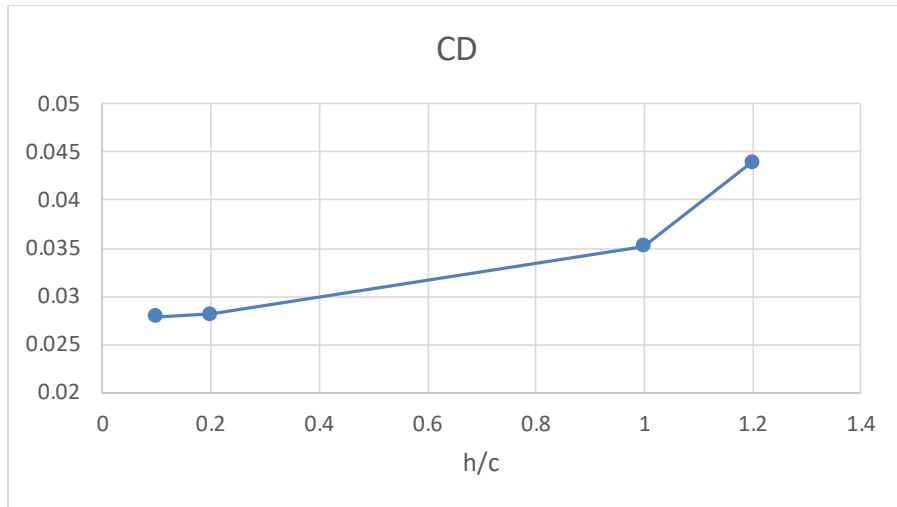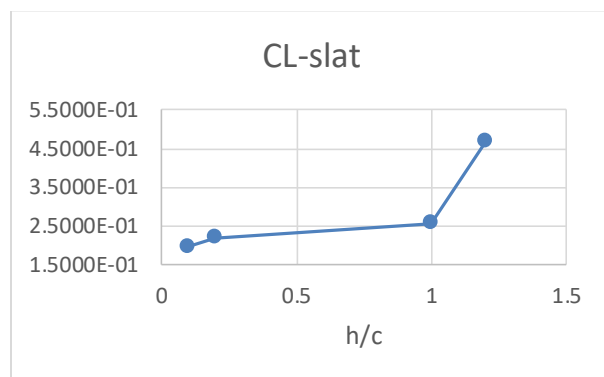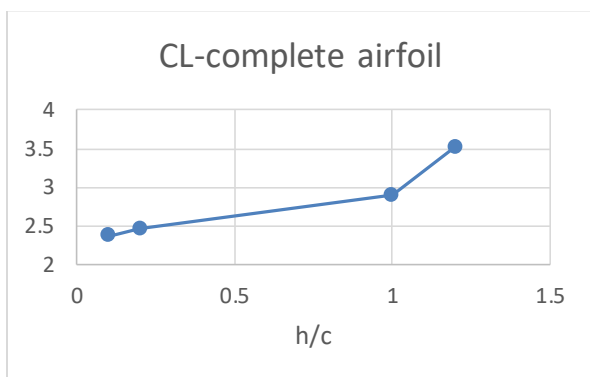Fig 4.2 Drag coefficient of 30P30N at different ride heights at freestream Mach number = 0.2

Lift and drag coefficient increase as the ground clearance increases. Figure 4.3 shows the change in lift coefficient of the slat, the main wing and the flap. They all show an increasing trend with ride height. The relative increase in the lift of the flap is the largest, and that of the slat is the smallest for h/c<1.
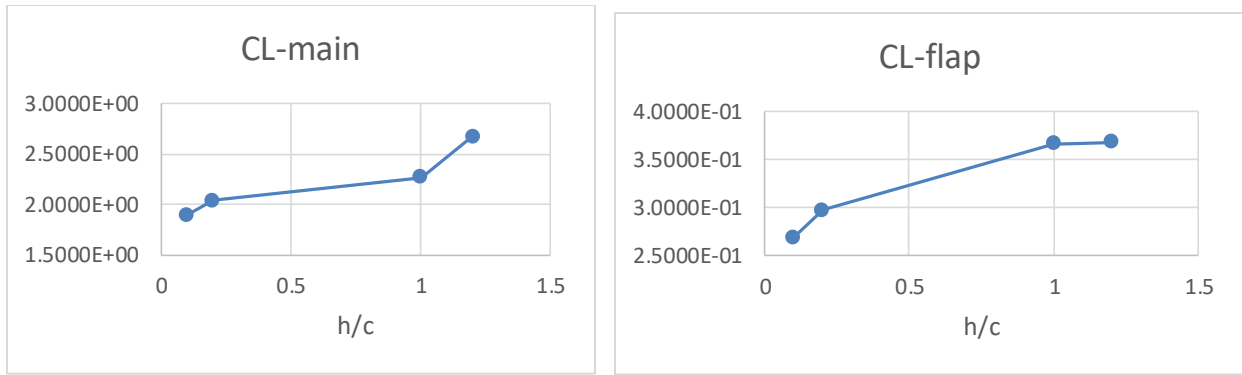
Fig 4.3 Lift coefficient of complete airfoil, slat, main and flap of 30P30N at different ride heights with freestream Mach number = 0.2

4.2 Pressure Coefficients and Contours

Figure 4.4 shows the pressure coefficient distributions at different ride heights.
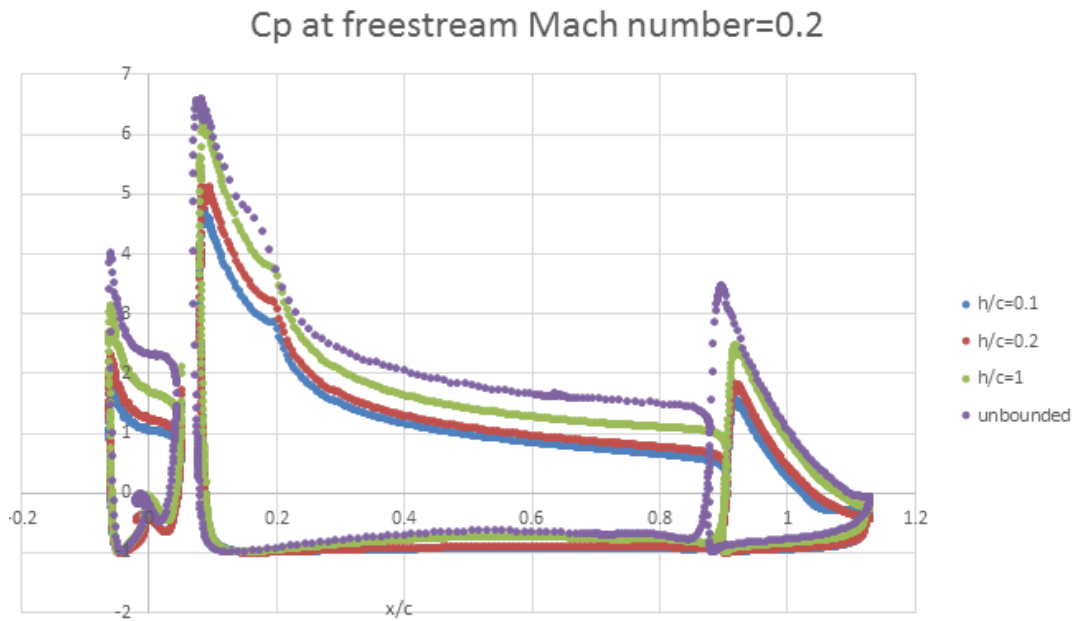
Fig 4.4 Pressure coefficient distributions at different height when freestream Mach number is 0.2

As the ground clearance decreases, the pressure coefficient on the upper surface increases. In particular, the upper surface pressure coefficient of slat, main wing and flap increases significantily, but the lower surface pressures coefficient increase only slightly on slat, main wing and flap. The position of the suction peak of each element hardly changes with increase in

21

ride height. Thus for a multi-element airfoil, the lift decreases significantly in GE compared to unbounded flow because of decrease in suction on the upper surface.

Figure 4.5 shows the pressure coefficient contours at h/c=0.1, 0.2 and 1.

Fig 4.5 Pressure coefficient contours at h/c=0.1, 0.2 and 1 for freestream Mach number = 0.2

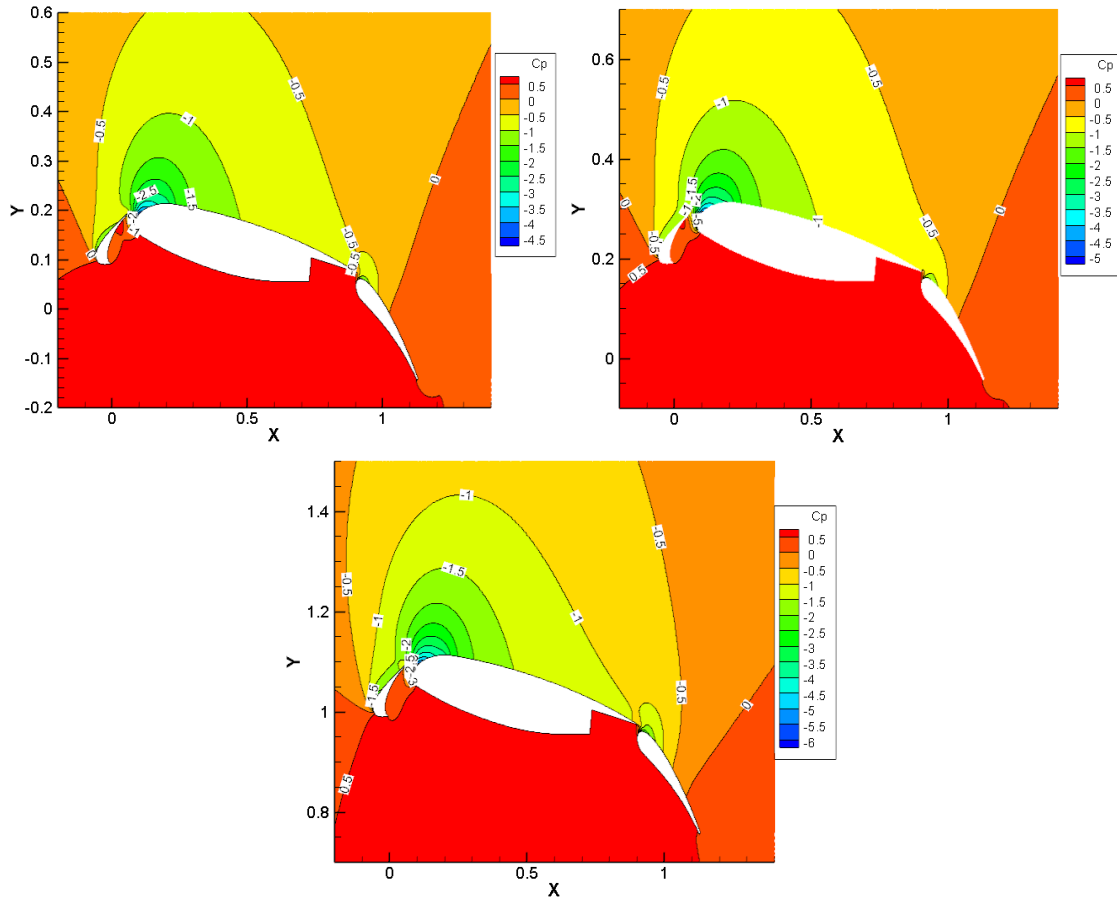The pressure coefficient at the lower surface remains almost the same at different ride height. The main factor for change in lift coefficient is the pressure coefficient on the upper surface. As the ground clearance increases, the upper surface pressure coefficient of slat, main wing and flap increases significantly, which implies a larger suction which leads to a lager lift coefficient. The minimum pressure coefficient points lie near the heading edge of slat, main wing and flap, the maximum pressure point lies on the lower surface. When ground clearance changes, the positions and of these points hardly change.

22

4.3 Velocity Contours

Figure 4.6 shows the velocity magnitude contours when h/c=0.1, 0.2 and 1.
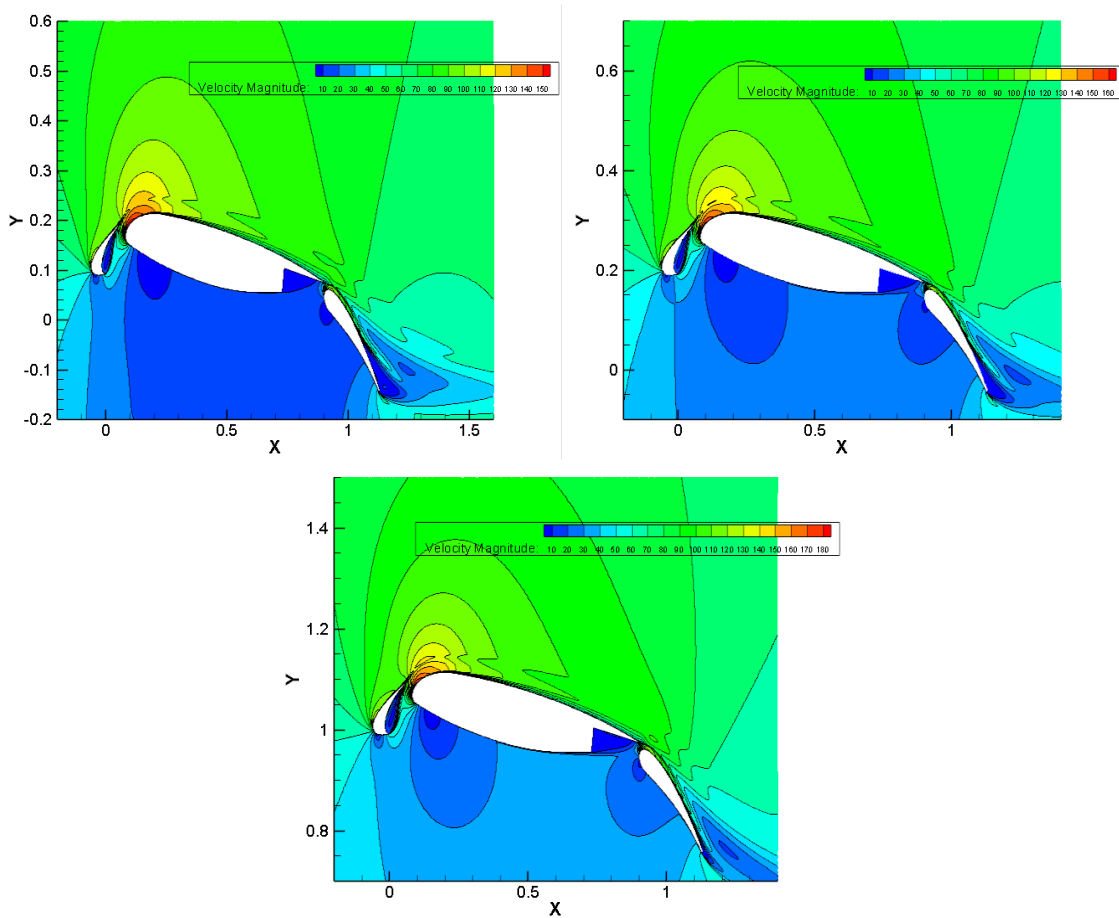
Fig 4.6 Velocity contours at h/c=0.1, 0.2 and 1 at freestream Mach number = 0.2

The velocity in the lower surface region is obviously lower than that in the upper surface region. The maximum velocity occurs at the head of main wing, the minimum velocity is on the lower surface. With decrease in ride height, the velocities in the lower and upper surface regions all decrease due to the ground blockage effect.

4.4 Streamlines

Figure 4.7 shows the streamlines around 30P30N at different ride heights h/c = 0.1, 0.2 and 1.

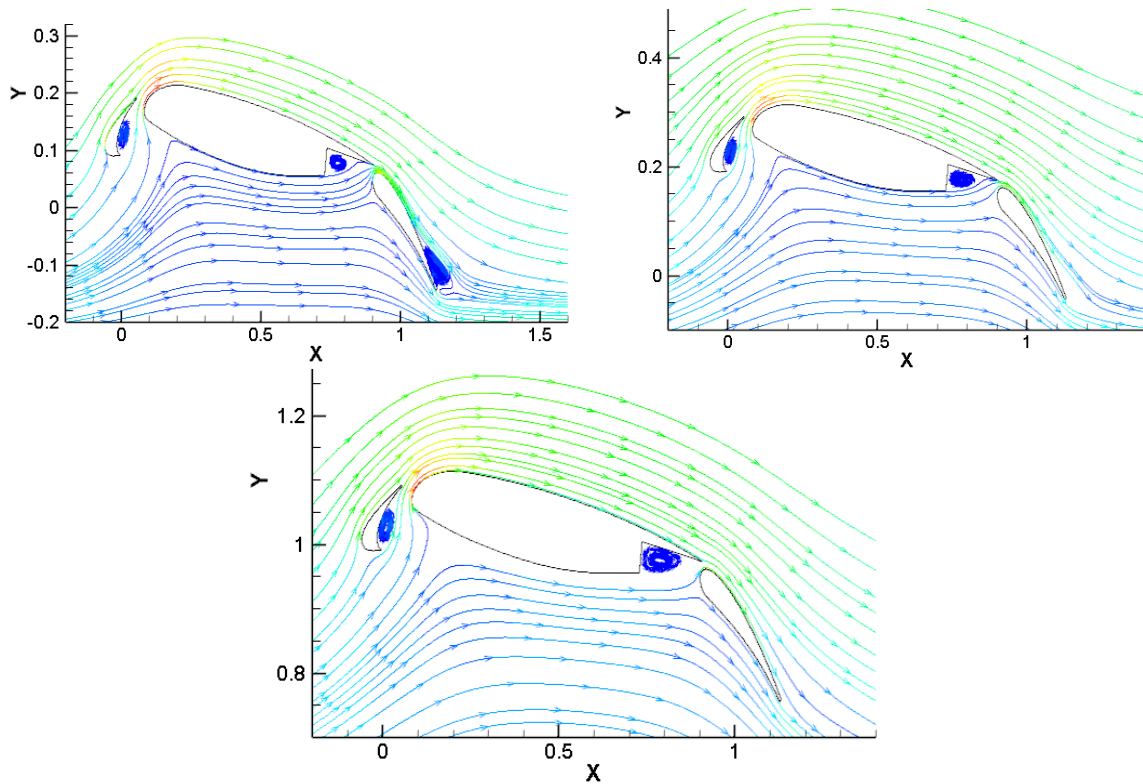Fig 4.7 Streamlines at h/c=0.1, 0.2 and 1 when freestream Mach number is 0.2

The boundary layers with high energy from on the main wing and the flap due to gaps, and improve the flow separation characteristics. The flow separation occurs on the flap in GE. As the ground clearance reduces, flow separates flow near the trailing edge of the flap.

4.5   Conclusions

In ground effect, the lift and drag coefficient increase as the ground clearance increases. Compared to unbounded flow, the decrease in lift results due to significant on the upper surface of the airfoil. The pressure increment on the lower surface of the airfoil is small. As the ground clearance decreases, the pressure coefficient increases because of decrease in suction on the upper surface. With the decreasing ride height, the velocities in the lower and upper regions surface decrease due to the ground blockage effect. At small ride height flow can separate near the trailing edge of the flap.

Chapter 5 Determination of Critical Mach Number of 30P30N in Ground Effect

5.1 Lift coefficient and drag coefficient

Figure 5.1 and Figure 5.2 show the change in lift coefficient and drag coefficient at various freestream Mach numbers with different ride heights. Lift curves show that at the same ride height, lift coefficient increases with Mach number before the critical Mach number and then decreases with Mach number after the critical Mach number. The reason for this behavior in lift curves was explained in Chapter 3. At the same ride height, when freestream Mach number changes from 0.2 to the critical Mach number, as the ride height increases the lift coefficient increases. However, when freestream Mach number increases from the critical Mach number to 0.5, lift coefficient decreases. It can be noticed from Figure 5.1 that the slope of lift curve is largest is unbounded flow compared that to ground effect. However, the slopes pf the lift curves as well as the magiyudes of lift coefficients change very little for Mach number. Drag curves show that at the same height, drag coefficient remians almost the same at Mach number less than the critical Mach number and then increases sharply with Mach numbers greater than the critical Mach number. At the same freestream Mach number, drag coefficient decreases as the ground clearance decreases. Curves of lift and drag coefficient at ride height 0.1 and 0.2 are very close, since the ground clearances are very close.
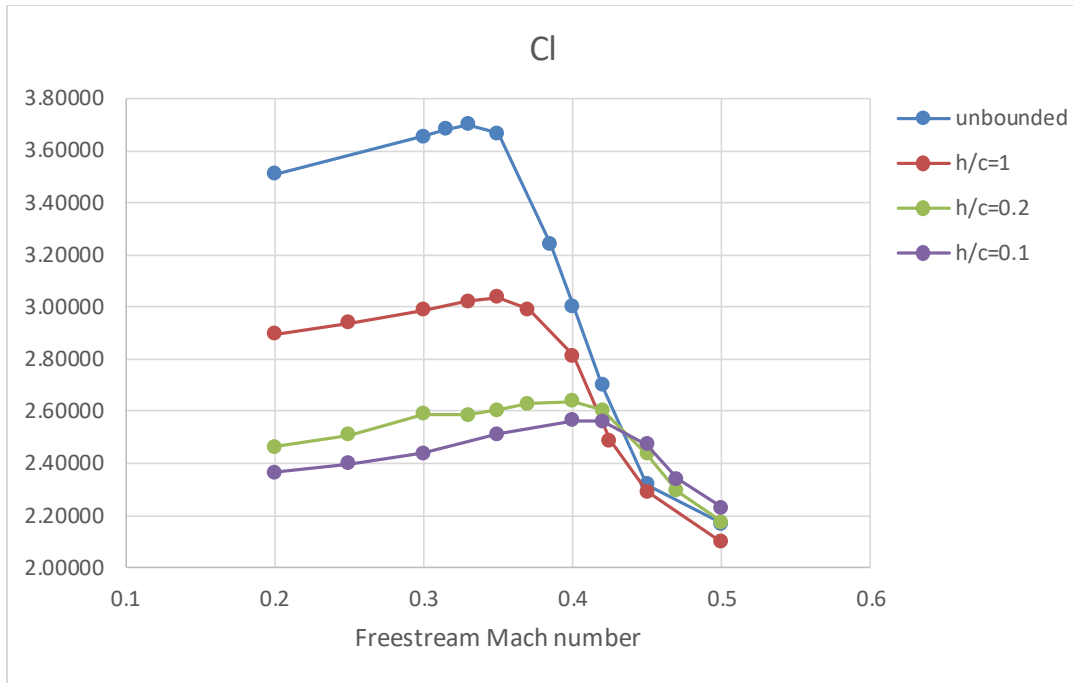
Fig 5.1 Variation in lift coefficients of 30P30N with different freestream Mach number at different ride heights
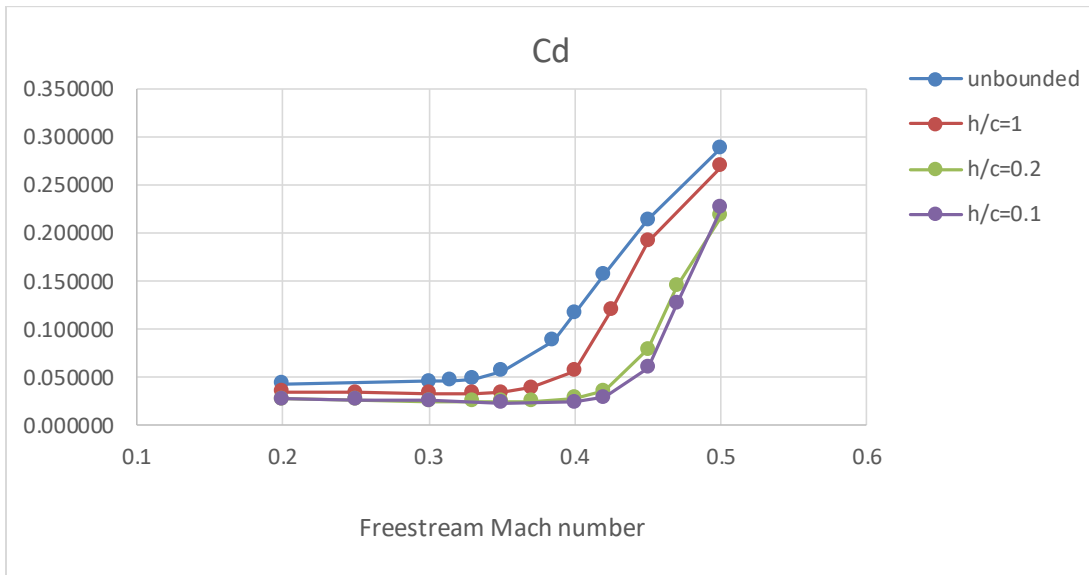

Fig 5.2 Variation in drag curves of 30P30N with different freestream Mach number at different ride heights

Figure 5.3 shows the change in lift coefficient with ride heights of h/c=0.1, 0.2, 1 and unbounded flow at varouis freestream Mach number. When freestream Mach number is small,

the viriation in lift coefficient with ride height has a similar trend and the lift coefficient increases with increasing ride height. However when freestream Mach number becomes larges, the lift coefficient decreases with increase in ride height as shown in Figure 5.3. Drag curves in Figure 5.4 show that for all freestream Mach numbers, the change in the drag coefficients with ride heights have similar trend.
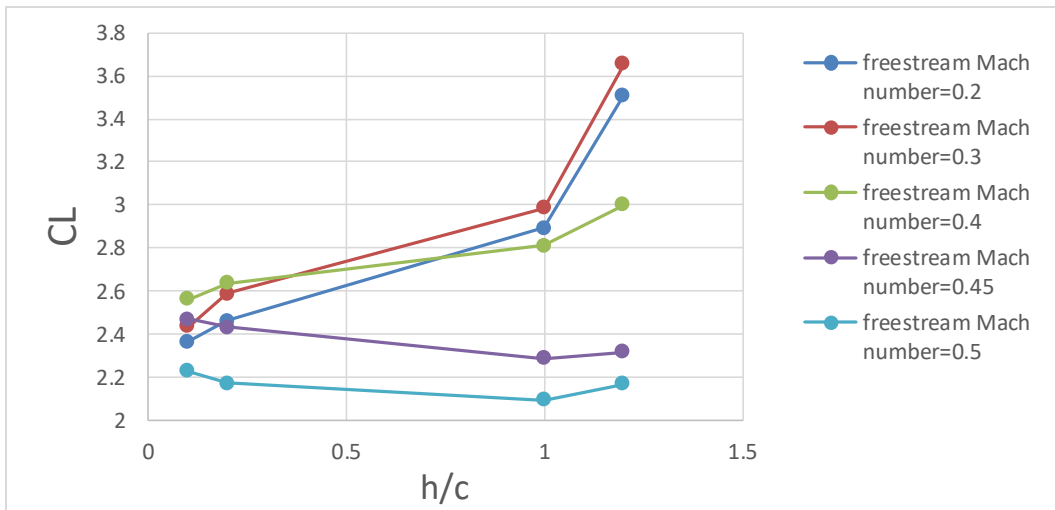

Fig 5.3 Variation in lift coefficient with ride height at various freestream Mach numbers
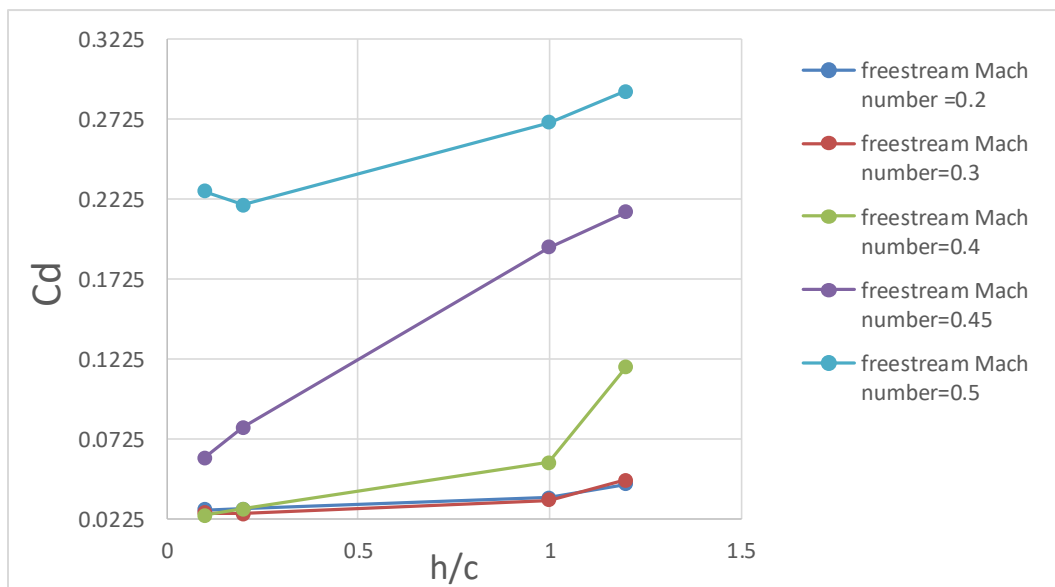

Fig 5.4 Variation in drag coefficient with ride height at various freestream Mach numbers

5.2 Pressure Coefficients and Contours

Figures 5.5-5.8 show respectively the pressure coefficient distributions at four freestream Mach number of 0.2, 0.3, 0.4, 0.5 at different ground clearances. As the ground clearance decreases, the pressure coefficient increases at low freestream Mach number of 0.2 and 0.3. At low freestream Mach number, the upper surface pressure coefficient of slat, main wing and flap increases significantly, however the lower surface pressure coefficient increases only slightly. For freestream Mach number less than 0.4, the pressure distribution is exhibit similar behavior in ground effect. However, when the freestream Mach number becomes greater than 0.4, the flow field becomes quite complex.
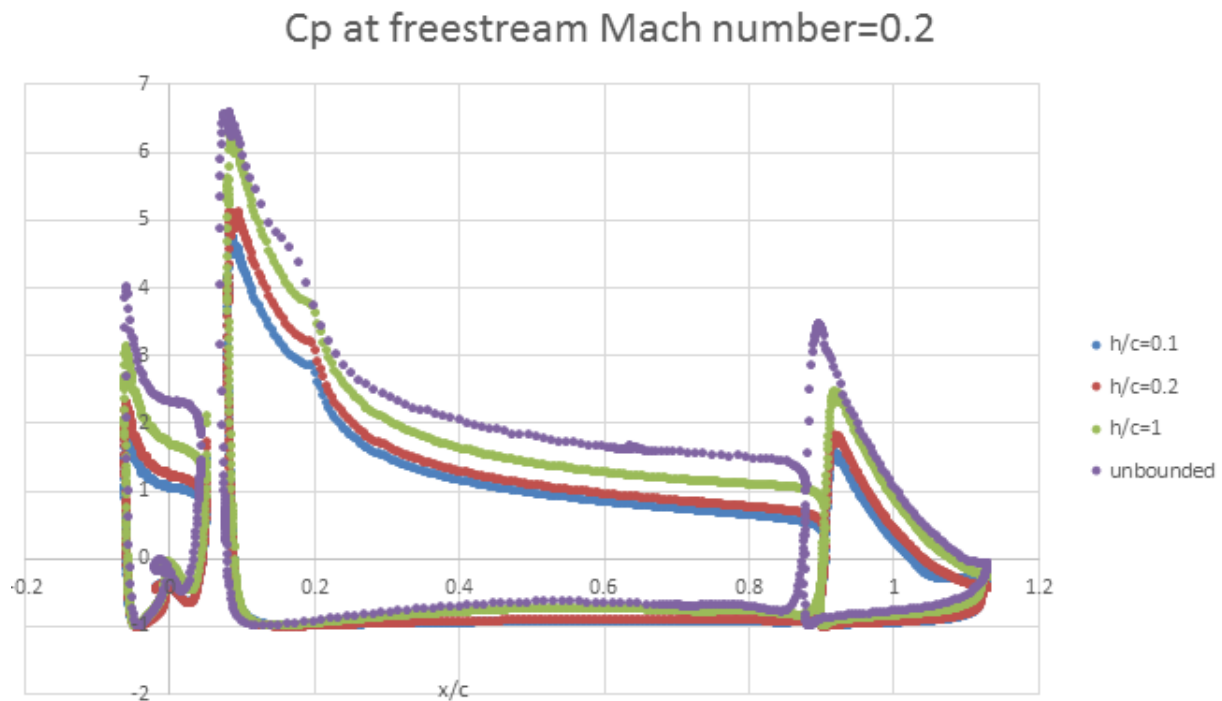

Fig 5.5 Pressure coefficient distributions at different heights at freestream Mach number = 0.2
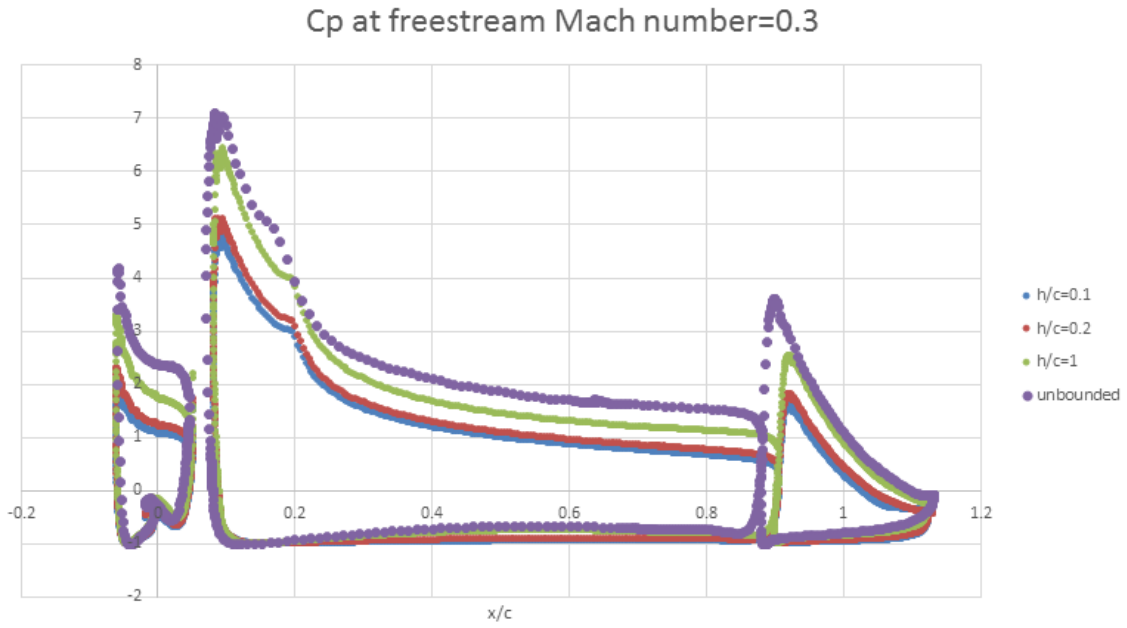
Fig 5.6 Pressure coefficient distributions at different heights at freestream Mach number = 0.3
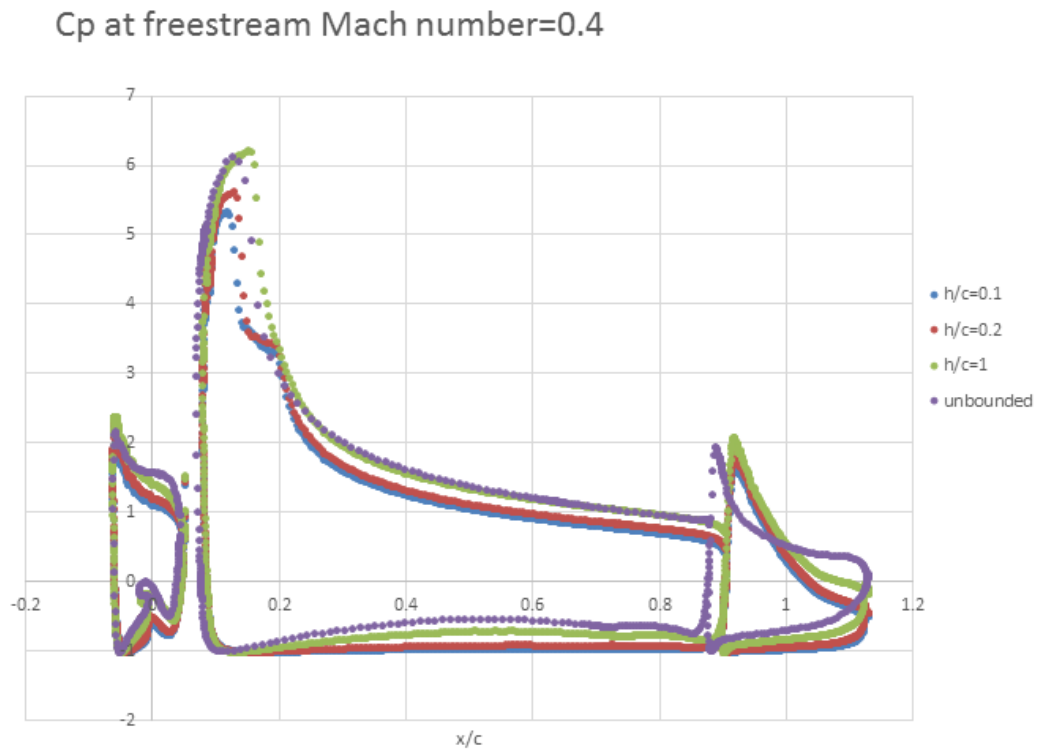

Fig 5.7 Pressure coefficient distributions at different heights at freestream Mach number = 0.4
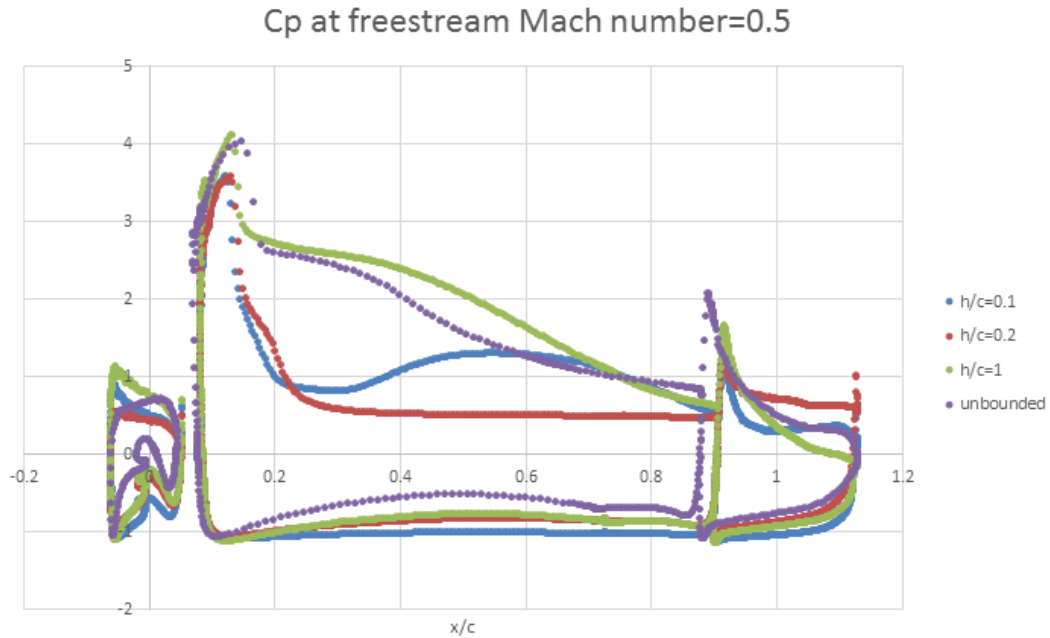
29

Fig 5.8 Pressure coefficient distributions at different heights at freestream Mach number = 0.5

5.3 Flow Field in Ground Effect at Freestream Mach Number 0.4

Figures 5.9 to 5.11 show the pressure coefficient contours, velocity magnitude contours and streamlines respectively at freestream Mach number 0.4 at varouis ride heights h/c=0.1, h/c=0.2, h/c=1 and unbounded flow.
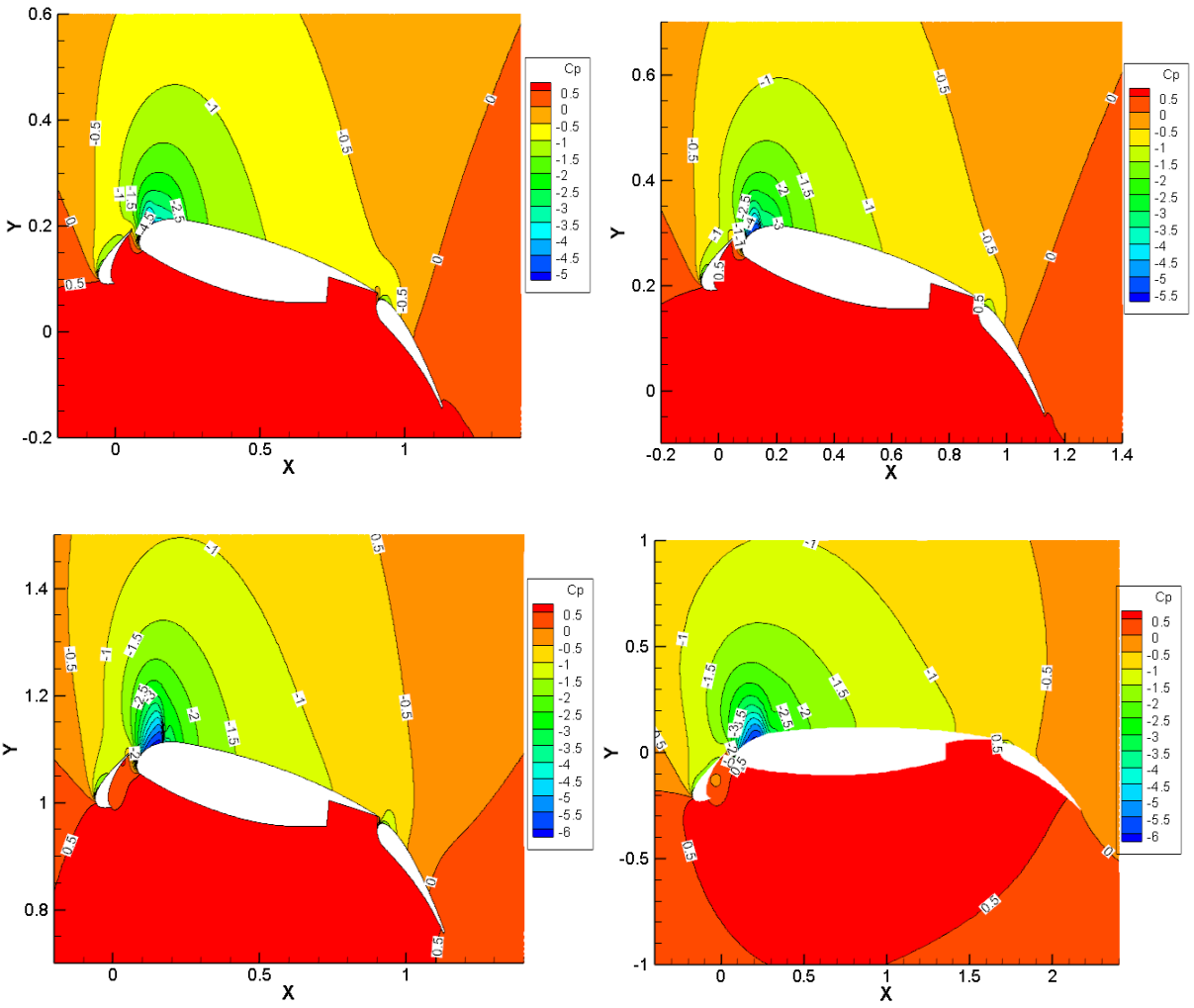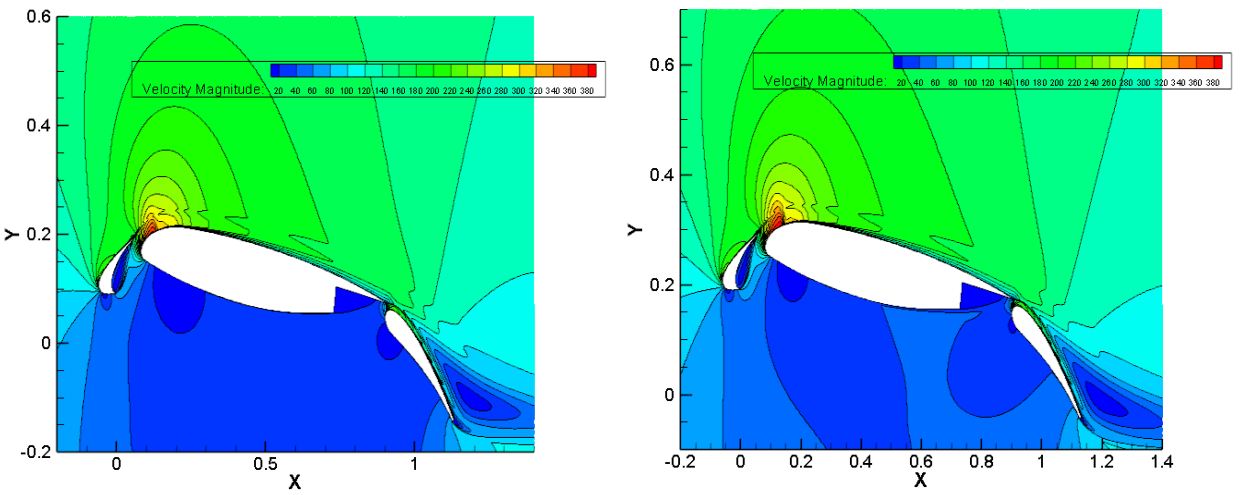
Fig 5.9 pressure coefficient contour when freestream Mach number is 0.4 at different height
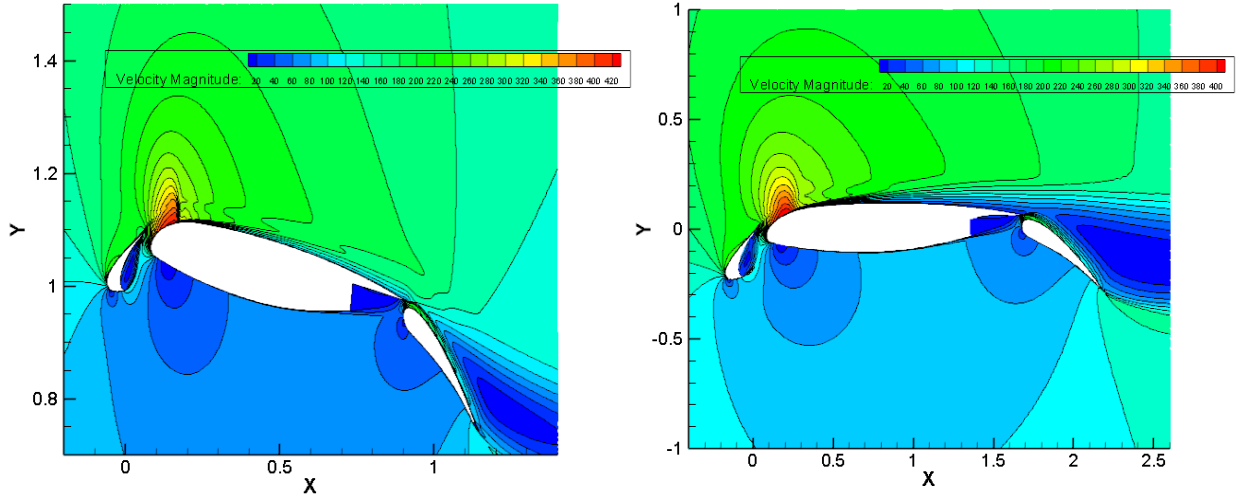
Fig 5.10 velocity magnitude contour when freestream Mach number is 0.4 at different height.
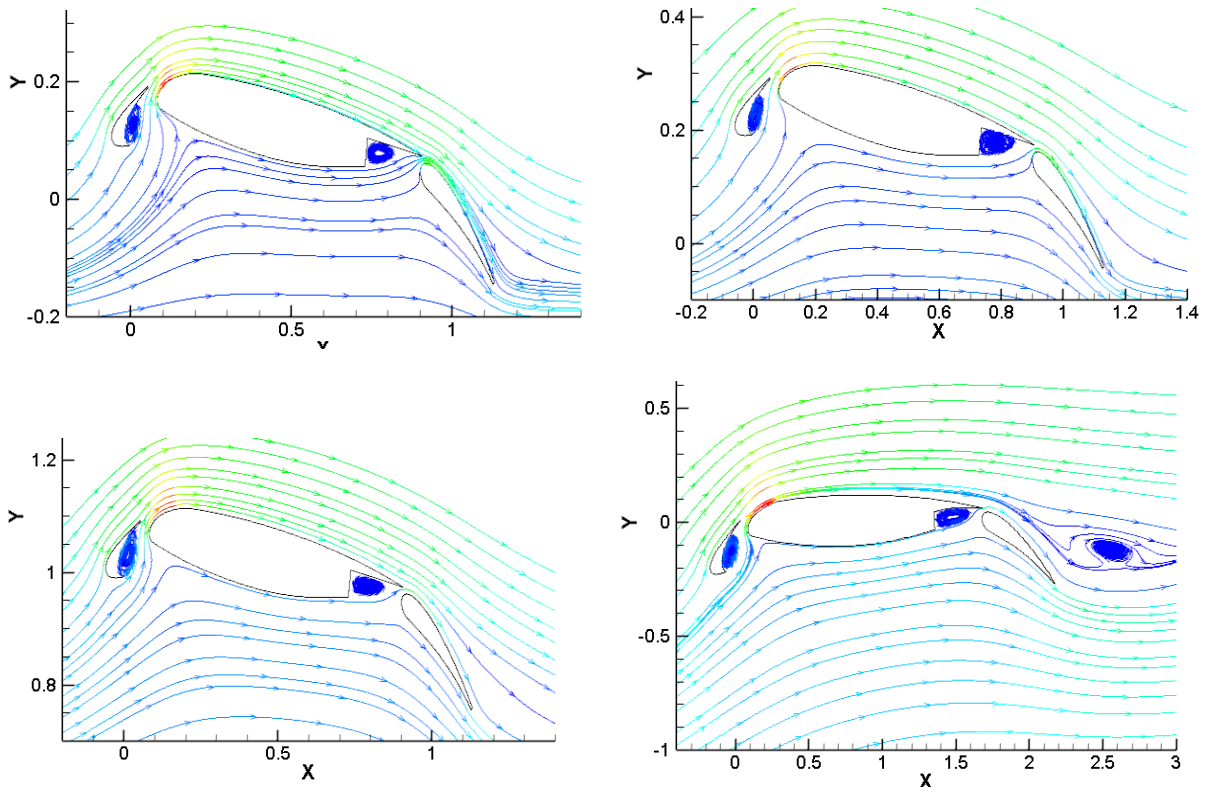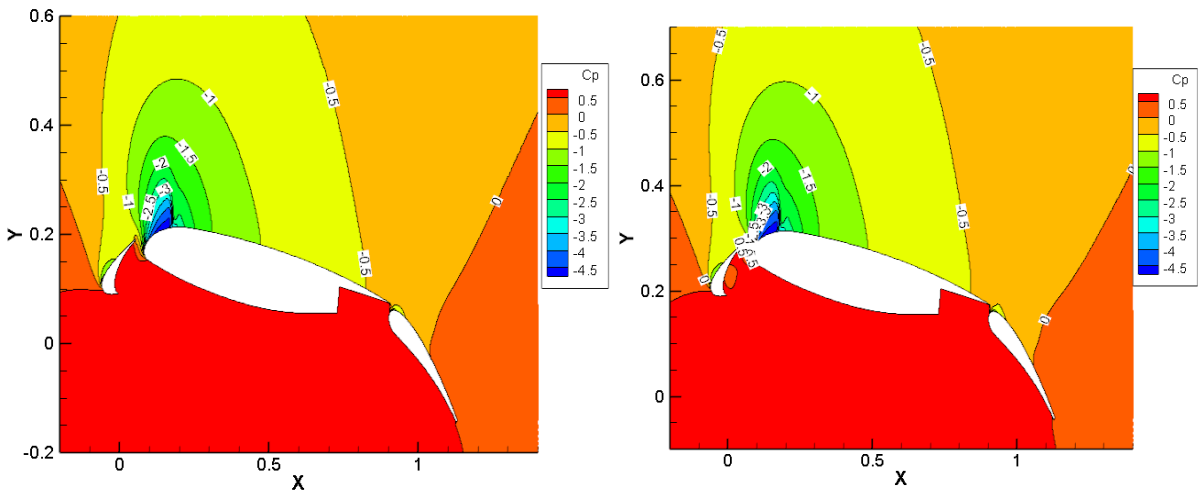

Fig 5.11 streamlines when freestream Mach number is 0.4 at different height

32

Although free stream Mach number 0.4 is greater than the critical Mach number in unbounded flow and at h/c=1, it is close to critical Mach number at h/c=0.2 and is less than the critical Mach number when h/c=0.1. Noting these changes in the critical Mach number with freestream Mach number and h/c, the behavior of pressure coefficient distribution and velocity distribution in Figure 5.9 and 5.10 can be explained. In Figure 5.11, there is separation on the flap in unbounded flow due to shock and boundary layer interaction.

5.4 Flow Field in Ground Effect at Freestream Mach number 0.45

Figures 5.12 to 5.14 show the pressure coefficient contours, velocity magnitude contours and streamlines respectively at free stream Mach number = 0.45 at various ride height h/c=0.1, h/c=0.2, h/c=1 and unbounded flow.
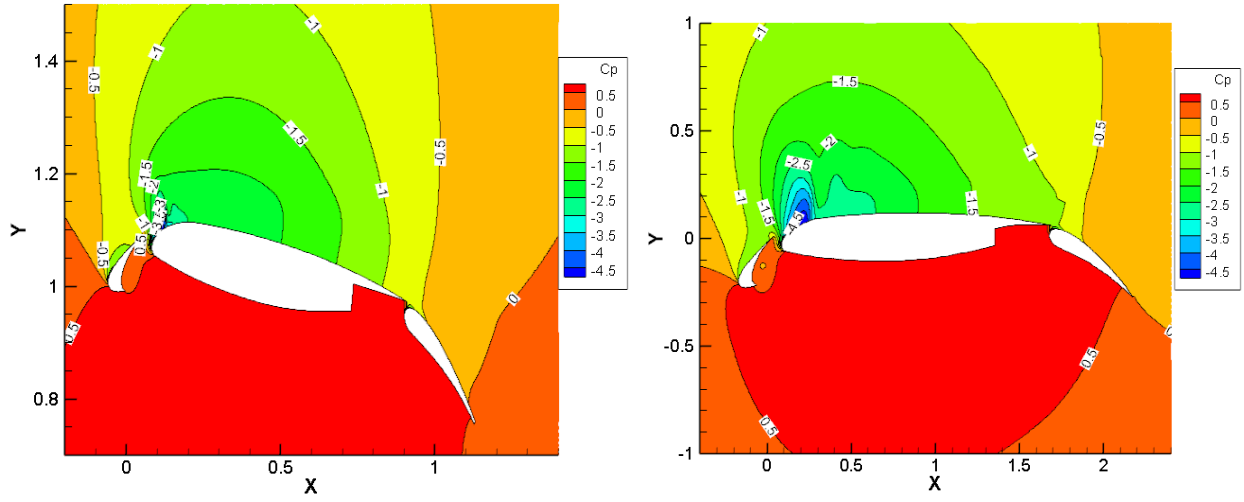
Fig 5.12 Pressure coefficient contours at freestream Mach number = 0.45 at different ride heights

Fig 5.13 Velocity magnitude contours at freestream Mach number = 0.45 at different ride heights.
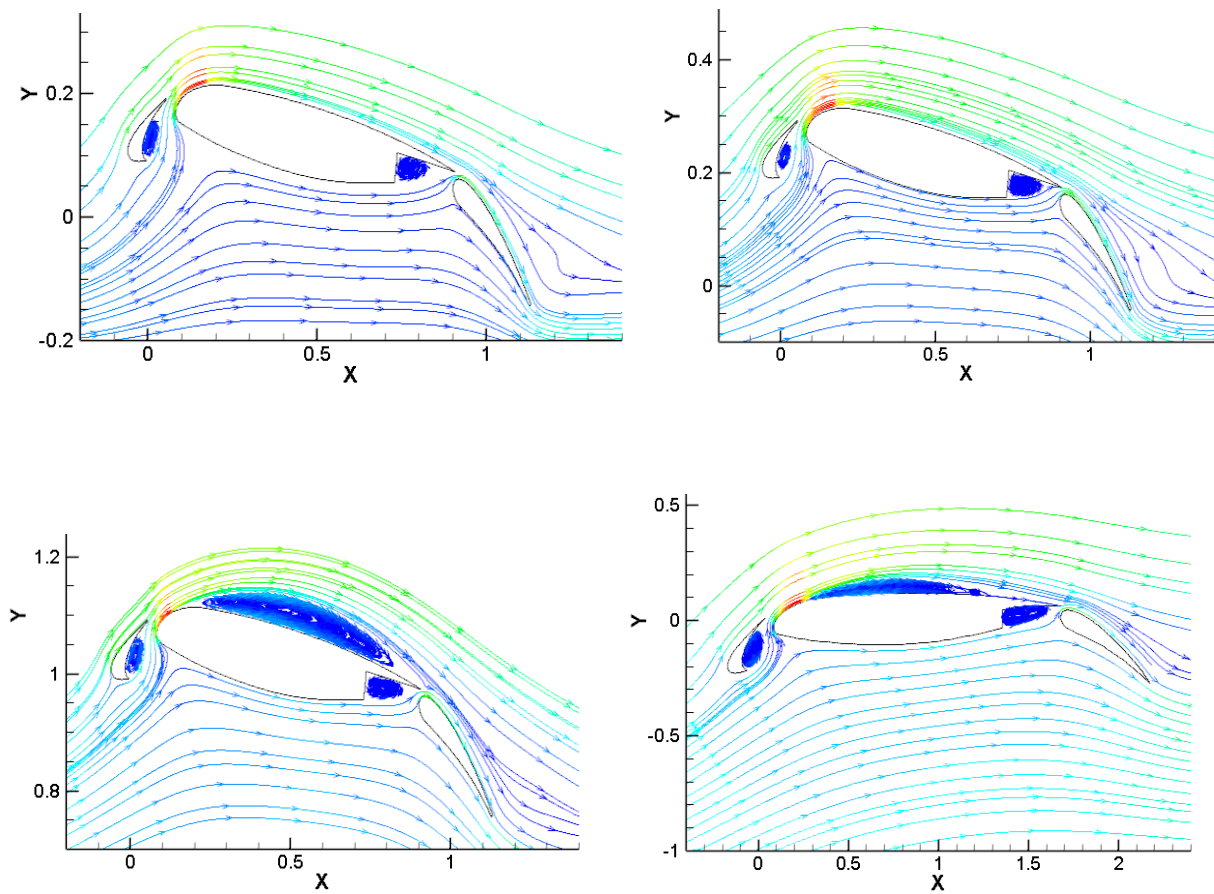
Fig 5.14 Streamlines at freestream Mach number = 0.45 at different ride heights

As the freestream Mach number increases from 0.4 to 0.45, there is strong shock and boundary layer interaction which influences both the pressure and velocity contours as can be seen from Figures 5.13 and 5.14. Figure 5.14 shows separation on the main wing at h/c=1 and in unbounded flow because of shock and boundary layer interaction when freestream Mach number is greater than the critical Mach number. However, when h/c=0.1 and h/c=0.2, freestream Mach number is very close to the critical Mach number and there is a weal shock at the leading edge of the main wing and the flow om the main wing is not separated.

5.5 Flow Field in Ground effect at Freestream Mach number 0.5

Figures 5.15 to 5.17 show the pressure coefficient contours, velocity magnitude contours and streamlines respectively at freestream Mach number 0.5 at various ride heights h/c=0.1, h/c=0.2 h/c=1 and unbounded flow.
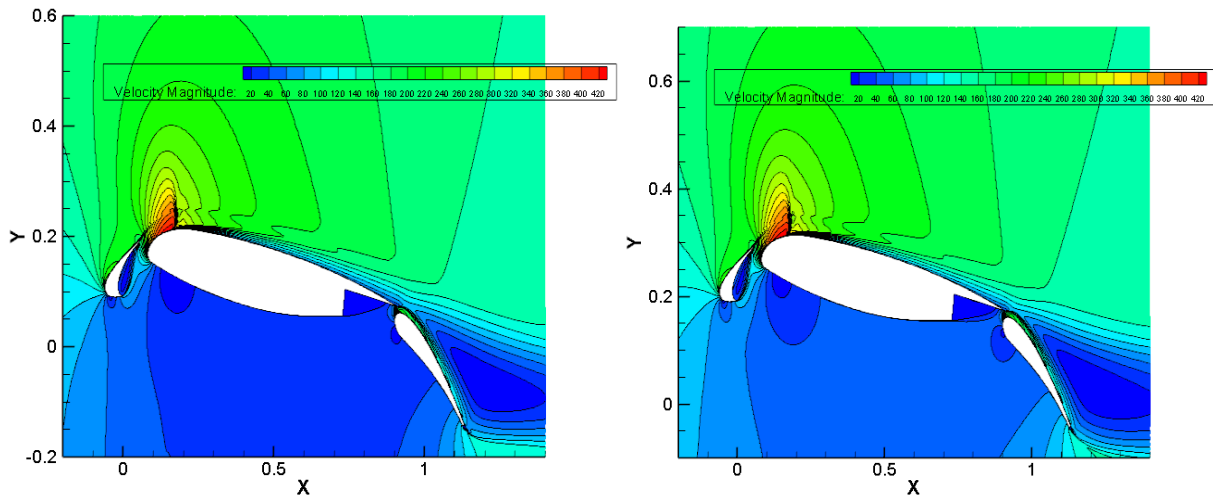
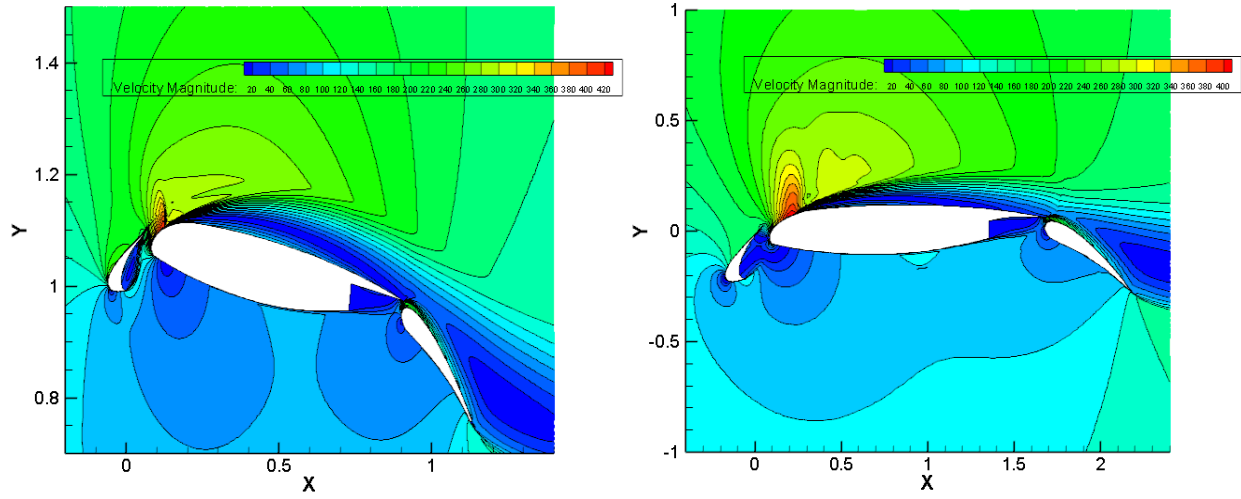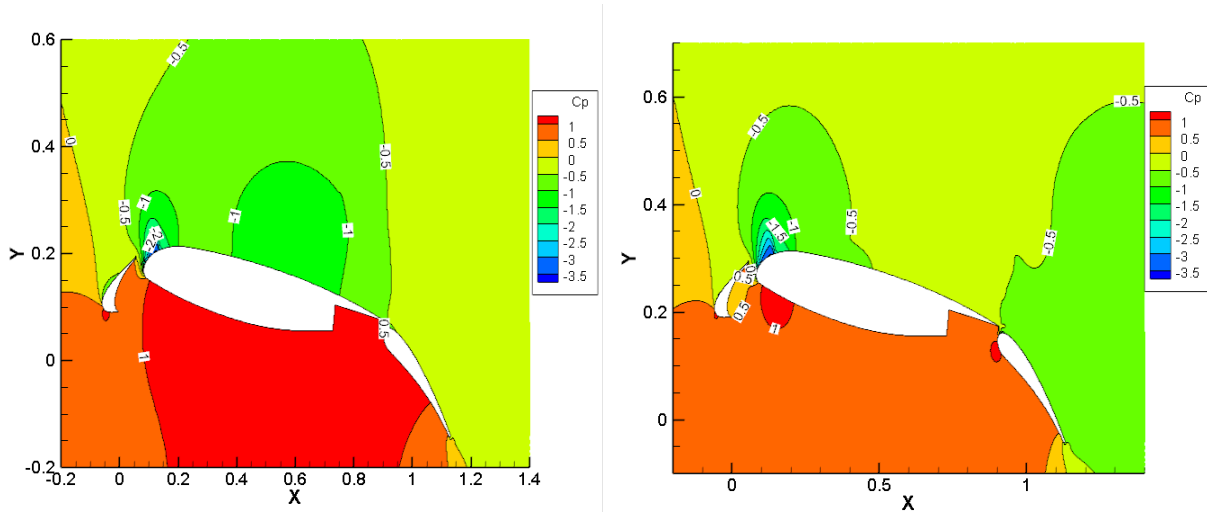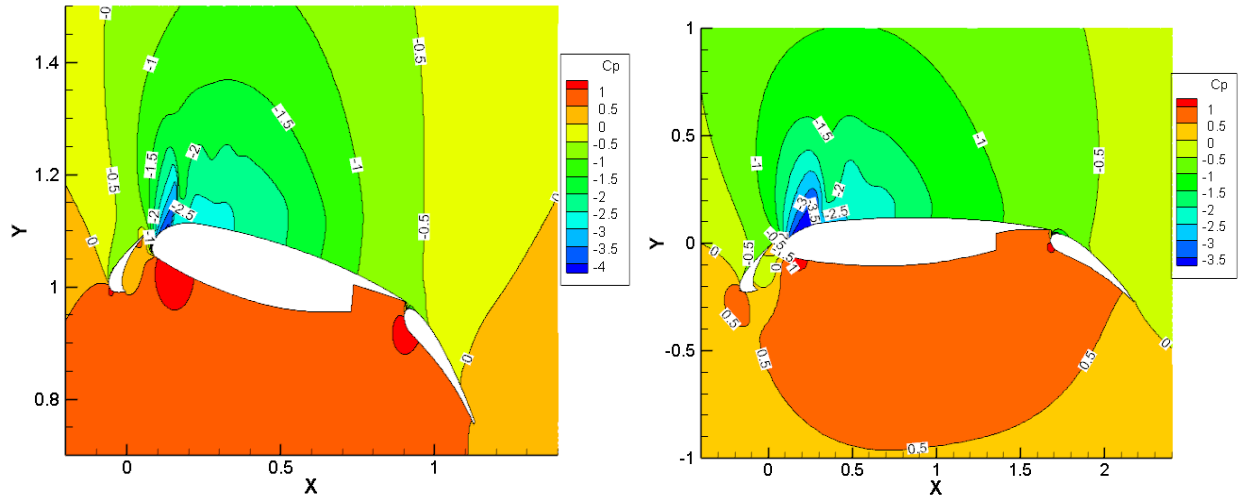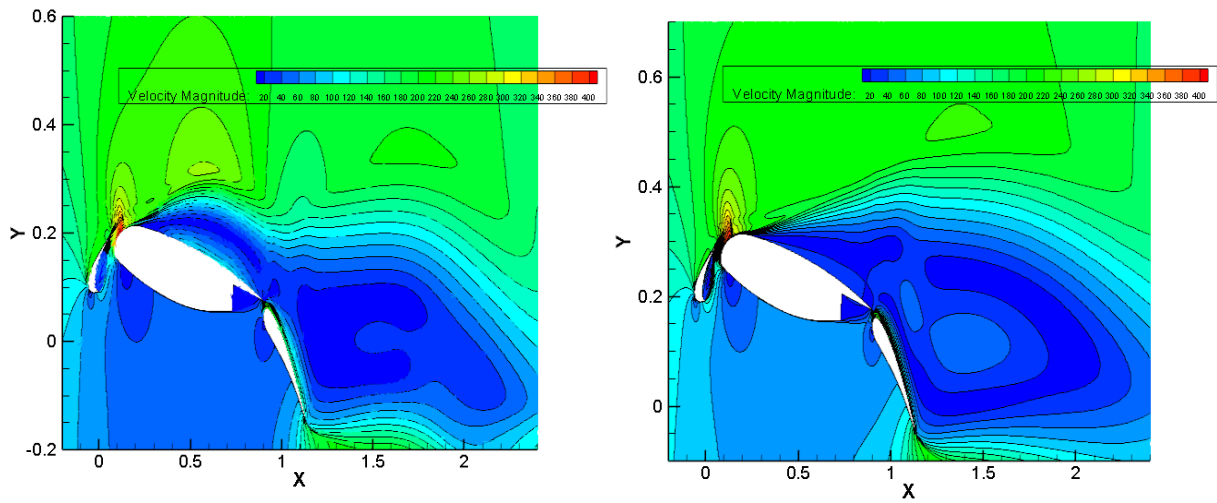Fig 5.15 Pressure coefficient contours at freestream Mach number = 0.5 at different ride heights
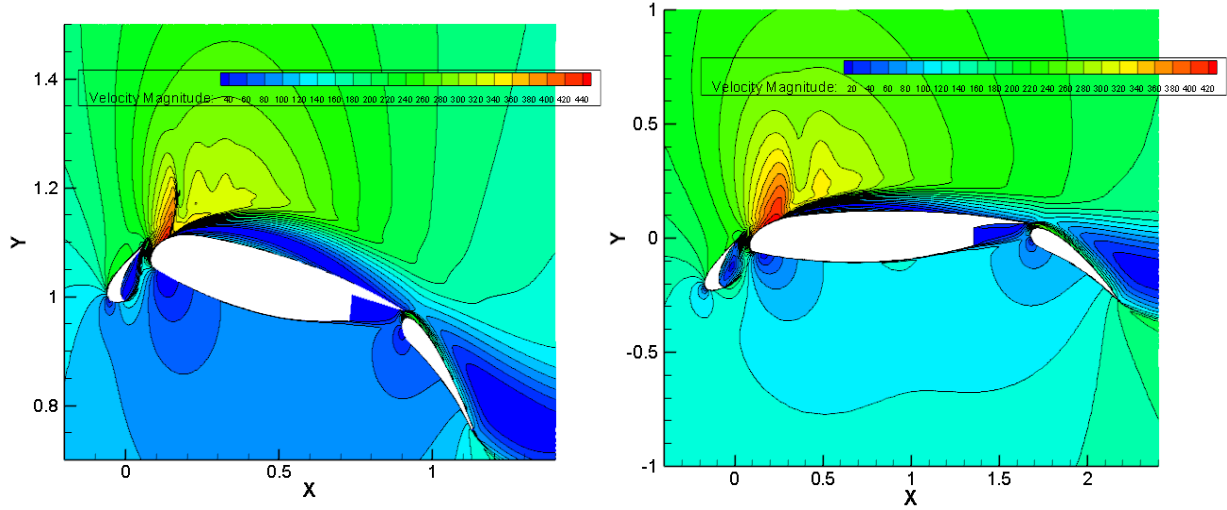
Fig 5.16 Velocity magnitude contours at freestream Mach number = 0.5 at different ride heights.
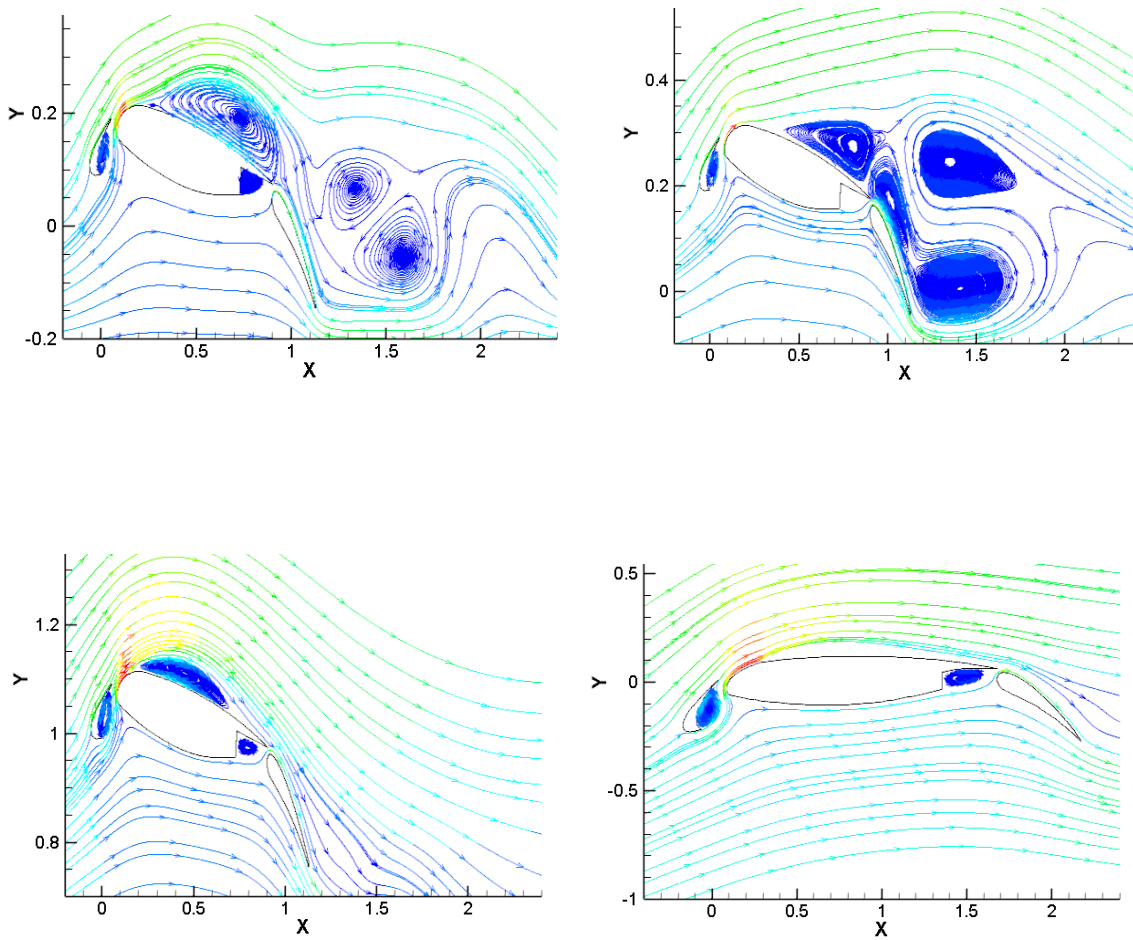

Fig 5.17 Streamlines at freestream Mach number = 0.5 at different ride heights

As the freestream Mach number increase to 0.5, it is much greater than the critical Mach number resulting in strong shoch and boundary layer interaction. The nature of pressure and velocity contours is similar to that in case of freestream Mach number 0.45. However, there is strong separation at h/c=0.1 and h/c=0.2. Figure 5.18 shows the variation in critical Mach number with ride height. Critical Mach number increases as the ride height decreases.
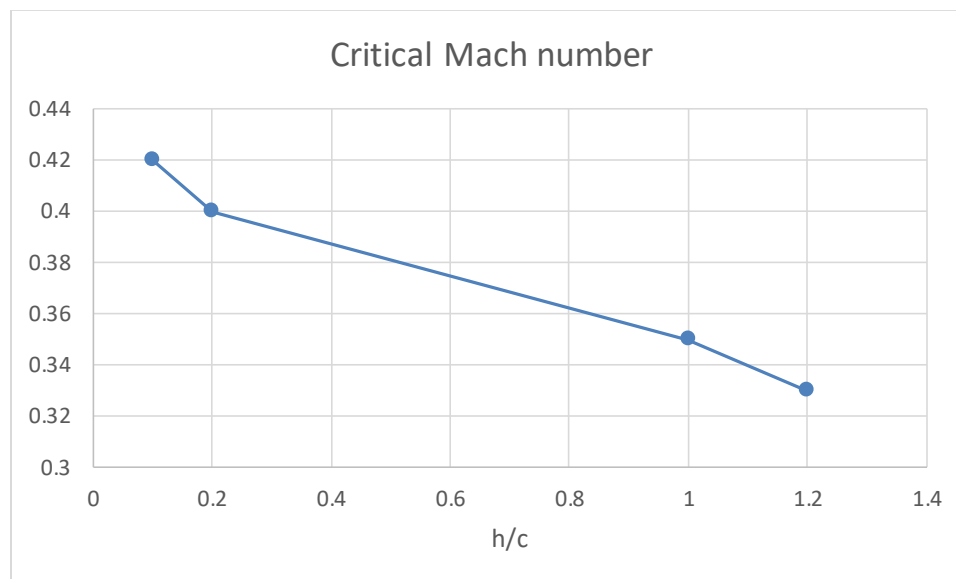
Fig 5.18 Variation in critical Mach numbers with ride height.

5.6   Conclusions

It has been demonstrated that the critical Mach number plays an important role in the nature of the flow field and aerodynamic properties of the airfoil. When the freestream Mach number is less than the critical Mach number, the lift coefficient increases with freestream Mach number while the drag coefficient remains almost the same. However when freestream Mach number is greater than the critical Mach number, due to the appearance of shock on the airfoil surface, the lift coefficient decreases with freestream Mach number and the drag coefficient dramatically

increases with freestream Mach number. The most important finding in ground effect is that as ride height decreases, the critical Mach number increases.

Chapter 6 Conclusions

1. Compared to the single element airfoil, multi-element airfoil has larger chord length and camber, and has gaps. In the unbounded flow, the larger chord length and camber increase the lift of airfoil from the potential flow viewpoint, and the flow in the gaps further increases the lift by delaying the flow separation form the viscous flow viewpoint.

2. In unbounded flow when the freestream Mach number is less than the critical Mach number, lift coefficient of 30P30N increases and then it decreases sharply when free stream Mach number is greater than the critical Mach number. The drag coefficient on the other hand remains same when freestream Mach number is less than the critical Mach number and then increases dramatically when freestream Mach number is larger than the critical Mach number.

3. In ground effect, the behavior of both the lift and drag coefficient is the same with respect to critical Mach number as described above for unbounded flow.

4. The critical Mach number increases with increase in ride height.

References

[1] Wang, Y., Wang, G. and Zhang, Y., "Study on Numerical Simulation of 30P30N Multi-Element Airfoil in Complex Flow Field," Acta Aerodynamic Asinica, Vol. 28, No.1, 2010.

[2] Coullietter, C., and Plotkin, A., "Aerofoil Ground Effect Revisited," Aeronautical Journal, No. 2121, 1996, pp. 65-74.

[3] Hsiun, C. M., and Chen, C. K., "Numerical Investigation of the Thickness and Camber Effects on Aerodynamic Characteristics for Two-Dimensional Airfoils with Ground Effect in Viscous Flow," Trans. Japan Soc, Aero. Space Sci., Vol. 38, 1994, pp. 78-90.

[4] Qu, Q. L., Wang, W., Liu, P. Q., and Agarwal, R. K., "Airfoil Aerodynamics in Ground Effect for Wide Range of Angles of Attack," AIAA Journal, Vol. 53, No. 4, 2015, pp. 1048-1061.

[5] Yang, W., Lin F., and Yang Z., "Investigation on Application of High-Lift Configuration to Wing-in-Ground Effect," Proceedings of the Institution of Mechanical Engineers, Part G: Journal of Aerospace Engineering, Vol. 226, No.3, 2012, pp. 260-271.

[6] Carter, A. W., "Effects of Ground Proximity on the Longitudinal Aerodynamic Characteristics of an Un-Swept Aspect-Ratio-10 Wing," NASATN-D-5662, 1970.

[7] Chen, H. et al. "GA Optimization Design of Multi-Element Airfoil," Seventh International Conference on Computational Fluid Dynamics (ICCFD7), 2012.

[8] Pascioni, K., Cattafesta, L. N., and Choudhari, M. M., "An Experimental Investigation of the 30P30N Multi-Element High-Lift Airfoil," 20th AIAA/CEAS Aeroacoustics Conference, 2014.

[9] Rumsey, C. L. and Ying, S. X., "Prediction of High Lift: Review of Present CFD Capability," Progress in Aerospace Sciences, Vol. 38, No. 2, 2002, pp. 145-180.

[10] Spalart, P. R., and Allmaras, S. R., "A One-Equation Turbulence Model for Aerodynamic Flows," AIAA Paper 92-0439, Jan. 1992.

Vita

Bowen Hu

Degrees   M.S. Mechanical and Aerospace Engineering, May 2017
B.S. Material Science and Engineering, June 2015

Birth of Place   Wuhan, Hubei, China

Publications   Bowen Hu, Qiulin Qu, and Ramesh K. Agarwal, "Numerical Determination of Critical Mach Number of a Three-Element Airfoil in Unbounded Flow and in Ground Effect,"

AIAA 2018 SciTech Forum, Kissimmee, Florida, 8-12 January 2018.

May 2017